Journal Pre-proof

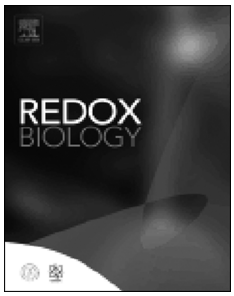

Oxidative Stress-Induced Endothelial Dysfunction Drives Mechanical and Infectious Lung Injury: Therapeutic Potential of Kaempferol in Males

Ziqi Shang, M.S., Zhiye Guo, Ph.D., Wen Tian, M.D., Ph.D., Feixiang Zhu, Ph.D., Tao Jiang, M.S., Weiyi Hu, Ph.D., Qingping Yao, Ph.D., Yunlong Huo, Ph.D., Yingxin Qi, Ph.D., Hanqin Wang, Ph.D., Kai Huang, Ph.D.

PII: S2213-2317(26)00197-7

DOI: https://doi.org/10.1016/j.redox.2026.104199

Reference: REDOX 104199

To appear in: *Redox Biology*

Received Date: 22 February 2026

Revised Date: 15 April 2026

Accepted Date: 1 May 2026

Please cite this article as: Z. Shang, Z. Guo, W. Tian, F. Zhu, T. Jiang, W. Hu, Q. Yao, Y. Huo, Y. Qi, H. Wang, K. Huang, Oxidative Stress-Induced Endothelial Dysfunction Drives Mechanical and Infectious Lung Injury: Therapeutic Potential of Kaempferol in Males, *Redox Biology*, https://doi.org/10.1016/j.redox.2026.104199.

This is a PDF of an article that has undergone enhancements after acceptance, such as the addition of a cover page and metadata, and formatting for readability. This version will undergo additional copyediting, typesetting and review before it is published in its final form. As such, this version is no longer the Accepted Manuscript, but it is not yet the definitive Version of Record; we are providing this early version to give early visibility of the article. Please note that Elsevier's sharing policy for the Published Journal Article applies to this version, see: https://www.elsevier.com/about/policies-and-standards/sharing#4-published-journal-article. Please also note that, during the production process, errors may be discovered which could affect the content, and all legal disclaimers that apply to the journal pertain.

© 2026 Published by Elsevier B.V.

Journal Pre-proof

Oxidative Stress-Induced Endothelial Dysfunction Drives Mechanical and Infectious Lung Injury: Therapeutic Potential of Kaempferol in Males

Ziqi Shang[1#], M.S., Zhiye Guo[1#], Ph.D., Wen Tian[2#], M.D., Ph.D., Feixiang Zhu[1#], Ph.D., Tao Jiang[1,3], M.S., Weiyi Hu[1], Ph.D., Qingping Yao[1], Ph.D., Yunlong Huo, Ph.D., Yingxin Qi[1], Ph.D., Hanqin Wang[4*], Ph.D., Kai Huang[1,5*], Ph.D.

[#]The authors contributed equally to this study

1. Institute of Mechanobiology & Medical Engineering, School of Life Sciences & Biotechnology, Shanghai Jiao Tong University, 800 Dongchuan Road, Minhang, 200240, Shanghai, China

2. Department of Vascular Surgery, Intervention Center, Shanghai General Hospital, Shanghai Jiao Tong University School of Medicine, 200080, Shanghai, China

3. Key Laboratory for Biomechanics and Mechanobiology of Ministry of Education, School of Biological Science and Medical Engineering, Beihang University, Beijing, 100083, China

4. Translational Medicine Research Center, Suizhou Hospital, Hubei University of Medicine, Suizhou, 441300, Hubei, China

5. Key Laboratory for the Genetics of Developmental and Neuropsychiatric Disorders, Ministry of Education, Shanghai Jiao Tong University, 800 Dongchuan Road, Minhang, 200240, Shanghai, China

***Address correspondence to:**

Hanqin Wang, M.D., Ph.D.

Journal Pre-proof

Translational Medicine Research Center, Suizhou Hospital, Hubei University of Medicine, Suizhou 441300, China
Email: hanqin.wang@hbmu.edu.cn

Kai Huang, Ph.D.
Institute of Mechanobiology & Medical Engineering, School of Life Sciences and Biotechnology, Shanghai Jiao Tong University, 800 Dongchuan Road, Minhang, 200240, Shanghai, China.
Email: huang_kai@sjtu.edu.cn

Word Count Total (excluding cover page, references and figure legends): 10741
Word Count Abstract: 231
Number of Figures:10
Number of Tables:0

Journal Pre-proof

Journal Pre-proof

Abstract

Mechanical ventilation (MV) remains an essential life-support strategy for patients with respiratory failure or critical illness. However, the mechanical stress generated during MV can lead to ventilator-induced lung injury (VILI). By integrating population-level epidemiology with bulk microarray and single-cell transcriptomic profiling, we identify a convergent pathogenic program shared by MV- and sepsis-associated lung injury, characterized by persistent oxidative stress and widespread endothelial dysfunction. In the National Health and Nutrition Examination Survey (NHANES), higher dietary intake of kaempferol, a plant-derived flavonol, was associated with improved pulmonary function in men. Ingenuity Pathway Analysis (IPA) results showed that NADPH oxidase (NOX) in the plasma membrane is the direct target of kaempferol. AlphaFold Protein Structure Database and cryo-electron microscopy (cryo-EM) resolved NOX2 structure, combined with molecular docking, suggest a direct interaction between kaempferol and NOX2. We also found that MV led to elevated reactive oxygen species (ROS) and induced endothelial dysfunction in various regions of the lung. Of note, kaempferol alleviates abnormal mechanical stress-induced ROS and endothelial barrier disruption by inactivating NOX2-Calcium-calmodulin-dependent protein kinase II (CaMKII)-Extracellular signal-regulated protein kinase 1/2 (ERK1/2) axis both in vivo and in vitro. Besides, kaempferol also improved survival rate and alleviated acute lung injury in cecal ligation and puncture (CLP)-induced septic mice via inhibiting the NOX2-CaMKII-ERK1/2 signaling pathway. These findings highlight the therapeutic potential of kaempferol in attenuating MV-associated lung injury and alleviating pre-existing inflammatory damage to the lung.

Keywords

Ventilator-induced lung injury; Critical care; Oxidative stress; Mechanical stress; Endothelial dysfunction; Reactive oxygen species; Dietary kaempferol

Highlights

- Microarray data and single-cell transcriptomics identify oxidative stress-induced endothelial dysfunction as common pathological drivers of lung injury promoted by mechanical ventilation (MV) and cecal ligation and puncture (CLP)

- Dietary kaempferol intake is positively associated with lung function parameters in men

- While MV-induced NOX2 upregulation drives oxidative stress and global endothelial dysfunction, kaempferol emerges as a therapeutic candidate by targeting ROS production at its source

- Kaempferol alleviates mechanical stress– and infection-induced lung injury through inhibition of the NOX2–CaMKII–ERK1/2 axis.

Graphical abstract

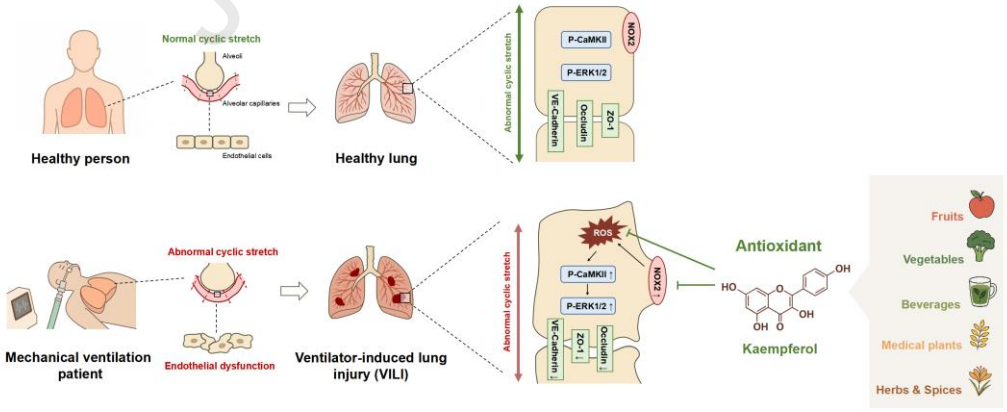

Journal Pre-proof

Journal Pre-proof

1. Introduction

Mechanical ventilation (MV) is a life-support treatment that helps or replaces breathing in patients with respiratory failure. It is used when oxygen levels are dangerously low or carbon dioxide levels are too high[1]. It is also required during general anesthesia to maintain safe breathing during surgery. MV is essential in intensive care units (ICUs) and operating rooms, saving lives in critical and surgical settings[1, 2]. However, MV can induce lung injury and inflammation—a phenomenon known as ventilator-induced lung injury (VILI)[3, 4]. The alveolar-capillary barrier, composed of endothelial and epithelial cells, is disrupted during VILI. This damage increases permeability, allowing protein leakage into alveoli and promoting leukocyte infiltration, further driving inflammation[5, 6]. To date, there is no specific pharmacological therapy for VILI[7]. Therefore, discovering the common molecular mechanisms of pre-existing lung injury and further damage caused by VILI will greatly benefit the prevention and treatment of endothelial dysfunction, vascular remodeling, and lung diseases.

Disruption of endothelial barrier integrity is a critical driver of vascular leakage in both VILI and sepsis-associated acute lung injury[5, 8-11]. One of the key drivers of endothelial dysfunction is oxidative stress[12-16], which arises from an imbalance between pro-oxidant forces and the antioxidant defense system. Abnormal mechanical stress-induced reactive oxygen species (ROS) generation triggers downstream signaling cascades that exacerbate endothelial dysfunction and promote pathological vascular remodeling[8, 17-19]. However, the molecular mechanisms through which MV-induced high cyclic stretch contributes to endothelial dysfunction and lung injury remain poorly understood, and the involvement of oxidative stress in this pathological cascade warrants further elucidation. Because oxidative stress is a central mechanism in VILI, The use of antioxidants may be a potential treatment for VILI. Previous studies have shown that antioxidant or redox-modulating agents,

including 4-octyl itaconate[20], amifostine[21], superoxide dismutase (SOD)[22], N-acetylcysteine[23], and quercetin[8], can mitigate experimental VILI, suggesting that targeting oxidative stress is a rational therapeutic strategy in this setting.

Kaempferol, a natural flavonol within the flavonoid family, exhibits potent antioxidant and anti-inflammatory properties[24, 25]. As a naturally occurring secondary metabolite, kaempferol is abundant in various fruits, vegetables, and herbal remedies, contributing to its dietary and therapeutic significance[25]. Numerous preclinical studies have demonstrated that kaempferol and its glycosides exhibit a broad spectrum of pharmacological properties, encompassing antioxidant, anti-inflammatory, antimicrobial, anticancer, cardioprotective, neuroprotective, antidiabetic, anti-osteoporotic, estrogenic/antiestrogenic, anxiolytic, analgesic, and antiallergic effects[25-27]. Despite kaempferol's documented anti-inflammatory and antioxidant properties, its efficacy in VILI remains unexplored, with critical gaps in understanding its impact on oxidative damage and pulmonary barrier integrity.

Here, we found that dietary kaempferol intake shows a positive association with enhanced lung function parameters, particularly in men. Microarray data and single-cell transcriptomic analyses reveal that oxidative stress and endothelial dysfunction serve as common pathological mechanisms underlying lung injury induced by both MV and CLP. Specifically, MV triggers NADPH oxidase 2 (NOX2) activation, leading to widespread oxidative stress and endothelial dysfunction. Notably, kaempferol emerges as a promising therapeutic agent by directly suppressing ROS production at its source. Furthermore, kaempferol effectively alleviates lung injury caused by mechanical stress or infection through inhibition of the NOX2-CaMKII-ERK1/2 signaling pathway, highlighting its potential as a dual-targeted intervention. As a naturally derived bioactive compound, kaempferol holds great potential for clinical translation in preventing VILI and other lung injuries.

2. Methods

2.1 Microarray data analysis

Transcriptomic datasets GSE226807 and GSE121550 were retrieved from the Gene Expression Omnibus database[28] (data acquisition via the R package GEOquery, v2.70.0) to identify differentially expressed genes (DEGs) in VILI and sepsis-induced lung injury models using the "limma" R package (v3.58.1). Functional characterization of these DEGs was performed through Gene Ontology (GO) enrichment and Gene Set Enrichment Analysis (GSEA) using the "clusterProfiler" package (v4.10.1) to explore the molecular impact of MV and sepsis on lung function. Detailed procedures, group definitions, and analysis thresholds are provided in Supplementary Method 2.1.

2.2 Single-cell RNA sequencing (scRNA-seq) analysis

The Seurat (v4.4.0) was employed to analyze scRNA-seq datasets derived from lung injury models induced by MV and CLP. Dimensionality reduction was performed using PCA, batch correction was performed by Harmony (v1.2.0)，and visualization was realized by uniform manifold approximation and projection (UMAP). After cell type annotation based on established lung cell markers[29-35], oxidative stress scores in endothelial cells were computed using AddModuleScore with the HALLMARK “REACTIVE_OXYGEN_SPECIES_PATHWAY” gene set. Detailed quality-control thresholds, clustering parameters, marker selection criteria, and gene-set retrieval procedures are provided in Supplementary Method 2.2.

2.3 Study population in NHANES

The National Health and Nutrition Examination Survey (NHANES), conducted by the National Center for Health Statistics in the United States, collects

demographic, socioeconomic, dietary, and health-related data for health assessment purposes. In this study, participants from the 2007-2010 NHANES surveys were considered as candidates, totaling 20,686 participants. After excluding samples with missing data on forced vital capacity (FVC) and forced expiratory volume in 1 second (FEV1), those diagnosed with COPD, individuals aged 20 years or younger, and samples with missing data on demographics, diabetes, BMI, bilirubin, and energy intake, a total of 5,587 samples were included. The specific process of participant selection is detailed in **Fig. 1**.

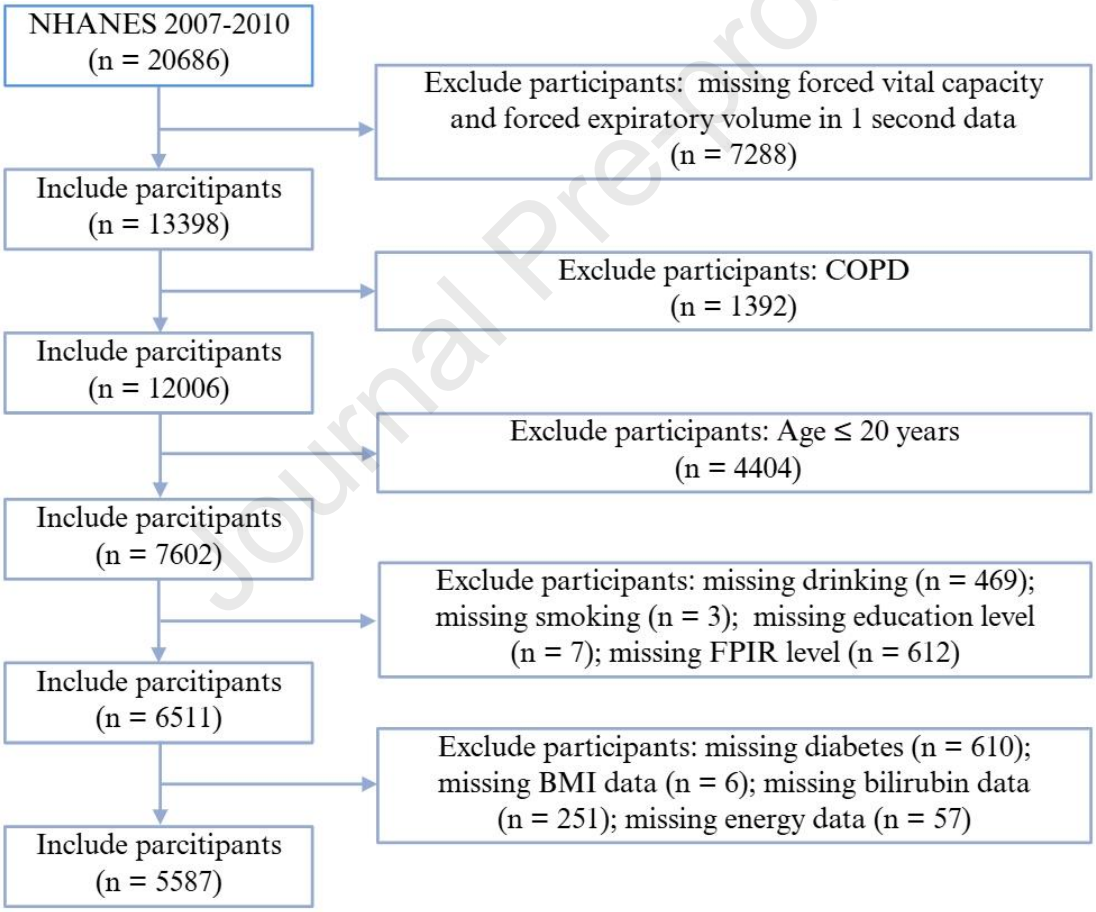

Figure 1. Participants screening flow chart.

2.4 Measurements of lung function parameters and PRISm definition

In this study, pulmonary function parameters such as FEV1 and FVC were obtained from the NHANES SPX dataset. The predicted values for each pulmonary function parameter were calculated using the NHANES III equations[36]. Cases of Preserved Ratio Impaired Spirometry (PRISm) were defined as those with an FEV1/FVC ratio ≥ 0.7 and an FEV1 percentage of predicted value < 80%[28].

2.5 Dietary kaempferol intake

The United States Department of Agriculture (USDA) Flavonoid Database provides comprehensive information on the dietary flavonoid content in various foods and beverages. Detailed data can be accessed at the following URL: https://www.ars.usda.gov/ARSUserFiles/80400535/Data/Flav/Flav3.3.pdf. This database includes the flavonoid content (mg/100 g) of all foods and beverages listed in the USDA Food and Nutrient Database for Dietary Studies (FNDDS), corresponding to the dietary data released by the What We Eat in America (WWEIA) survey and NHANES[37]. The dietary data from NHANES were collected through two non-consecutive 24-hour dietary recall interviews.

2.6 Collection of baseline features

Baseline characteristics, including demographics, lifestyle factors, and health status, were extracted from the NHANES demographic, questionnaire, and laboratory modules. Standardized clinical criteria were applied to define smoking and alcohol status, as well as the diagnosis of chronic conditions such as diabetes, hypertension, and hyperlipidemia. Detailed operational definitions and diagnostic thresholds for smoking status, alcohol consumption, diabetes, hypertension, and hyperlipidemia are provided in Supplementary Method 2.3.

2.7 Ingenuity Pathway Analysis (IPA)

Ingenuity Pathway Analysis (IPA) software (Version 145030503, Qiagen, Germany) leverages the Ingenuity Pathways Knowledge Database to interpret complex biological interactions, integrating curated data on genes, proteins, chemicals, and pathways for mechanistic analysis. It was used to identify functions and diseases related to kaempferol and analyze the top 30 molecules regulated by kaempferol. Furthermore, the distribution of these 30 molecules in different locations within the cell were presented by IPA.

2.8 Potential interaction between kaempferol and NOX2

The potential interaction between kaempferol and NOX2 was evaluated using the DeepMice platform, with protein structures retrieved from the AlphaFold database and the Protein Data Bank. Docking simulations were performed at predicted binding sites to assess binding orientations and affinities. The resulting molecular interactions were visualized and analyzed using PyMOL to identify key residues involved in the kaempferol-NOX2 complex. Detailed receptor or ligand preparation, and docking procedures are provided in Supplementary Method 2.4.

2.9 Animal studies

Male C57BL/6J mice were purchased from Zhejiang Vital River Laboratory Animal Technology Co., Ltd. All animals were housed under specific pathogen-free (SPF) conditions, maintained on a 12 h light/dark cycle, with ad libitum access to food and water. Allocation of mice and samples into groups was random. All procedures involving animals were approved by the Animal Ethics Committee of Shanghai Jiao Tong University and conducted in accordance with the Regulations for the Administration of Affairs Concerning Experimental Animals (Decree No. 55, 2001, Ministry of Health, China).

2.10 Animal models

Male C57BL/6 mice were subjected to mechanical ventilation (MV) for 4 hours at either low (9 mL/kg) or high (34 mL/kg) tidal volumes to establish the VILI model[8], with Kaempferol (15 mg/kg/day) administered as a 3-day pretreatment. For the sepsis-induced lung injury model, CLP was performed[13], and lung tissues were harvested 16 hours post-surgery. All procedures were conducted under appropriate anesthesia and temperature control, following established protocols for acute lung injury induction. Detailed VILI and CLP protocols are described in Supplementary Method 2.5.

2.11 Dihydroethidium (DHE) staining

The levels of ROS in lung tissue were assessed using dihydroethidium (DHE) fluorescence staining. Mouse lungs were embedded in optimal cutting temperature (OCT) compound and sectioned into 5 μm frozen slices. Human aortic endothelial cells (HAECs, immortalized) were seeded in confocal dishes and grown to approximately 70-80% confluence. After treatments, cells were fixed with 4% paraformaldehyde. Both the fixed HAECs and the prepared lung sections were incubated with freshly prepared DHE staining solution at 37°C for 30 minutes in the dark, followed by thorough washing with PBS. Fluorescent images were acquired using a confocal laser scanning microscope (Fluoview 1000, Olympus), and fluorescence intensity was quantified in ImageJ using mean fluorescence intensity.

2.12 Electron spin resonance determination of superoxide production in lung tissues and HAECs

The lung tissues were freshly harvested and homogenized in lysis buffer containing 1:100 protease inhibitor cocktail (Sigma-Millipore, USA), centrifuged at 12,000 rpm for 15 min. Protein content of the supernatant was determined using a protein assay kit (Bio-Rad). For HAECs, cells were collected in cold modified Krebs/HEPES (KHB) buffer after treatment. The

Journal Pre-proof

Electron spin resonance (ESR) was used to detect superoxide production. Detailed methods have been included in the Supplemental Materials.

2.13 Western blot

Total protein was extracted from lung tissues using RIPA buffer and separated via 10% SDS-PAGE before being transferred onto PVDF membranes. After blocking with 5% non-fat milk for 1 h, the membranes were incubated overnight at 4°C with specific primary antibodies. Following three washes with TBST, the membranes were incubated with corresponding HRP-conjugated secondary antibodies for 1 h at room temperature. Protein bands were visualized using enhanced chemiluminescence (ECL) reagents, and densitometric analysis was performed using ImageJ software for relative quantification. Primary antibody information and detailed western blot procedures are provided in Supplementary Method 2.6.

2.14 Immunofluorescence Imaging

Frozen lung sections were fixed, permeabilized, and incubated overnight with primary antibodies. After incubation with corresponding fluorescent secondary antibodies and DAPI nuclear staining, slides were mounted and visualized using confocal microscopy (Olympus Fluoview 1000). Primary antibody information and detailed procedures are provided in Supplementary Method 2.7.

2.15 Cell treatment

HAECs were obtained from QuiCell (Shanghai, China) and cultured in endothelial cell medium (ECM, QuiCell-Pri-8003) under standard conditions (37°C, 5% CO_2). To investigate the effect of ROS on cellular function, HAECs were treated with H_2O_2. After seeding the HAECs onto a six-well plate, cells

were allocated into three groups: the H_2O_2 group, in which cells were exposed to 100 μM H_2O_2 for 6 h; the kaempferol + H_2O_2 group, in which cells were pretreated with 10 μM kaempferol for 1 h followed by co-incubation with 100 μM H_2O_2 for 6 h; and the control group, in which cells received an equal volume of 0.1% DMSO for 6 h.

2.16 Cyclic Stretch Loading

Cells were subjected to cyclic stretch as previously described[8, 38-45]. Cyclic stretch was performed on human aortic endothelial cells (HAECs) using the FX5000 T Strain Unit (FlexCell International, USA) to simulate cell deformation during H-MV in vivo, with 20% stretch amplitude and 0.5 Hz frequency for 4 h. Then, HAECs were harvested for further examination.

2.17 Survival Curve

For survival analysis, mice were monitored every 30 min starting at 6 h post-CLP surgery to document mortality. Kaplan-Meier survival curves were generated using Prism software.

2.18 Lung Wet/Dry Weight Ratio

The lung wet/dry weight ratio was measured to assess pulmonary edema, reflecting endothelial permeability and injury severity. After excision, lungs were weighed (wet weight), dried at 60°C for 48 h, and re-weighed (dry weight) to determine the ratio.

2.19 Lung Evans Blue staining

To assess pulmonary endothelial permeability, an Evans Blue dye extravasation assay was conducted. A 2% Evans blue solution was prepared by dissolving 20 mg of Evans blue powder in 1 mL PBS. Mice were administered Evans blue (2%, 2 mL/kg) via tail vein injection and allowed to

circulate for 0.5 h. Afterward, animals were euthanized and perfused with PBS through the heart until the effluent from the right atrium was clear, after which the lungs were collected and photographed to document Evans blue staining.

2.20 H&E staining and histological analysis

Lung tissues were fixed in 4% paraformaldehyde (24 h), dehydrated in graded ethanol, cleared in xylene, and paraffin-embedded. Sections (5 μm) were cut and stained with H&E. Histopathological evaluation was performed under bright-field microscopy, with representative images captured.

2.21 Statistical analysis

For the NHANES study, survey-weighted models were applied using R (v4.3.3) to account for complex sampling designs. Categorical and continuous variables were compared using Rao & Scott-adjusted Chi-square and Kruskal-Wallis tests[46, 47], respectively, while multivariable linear and logistic regressions were constructed to evaluate the associations between kaempferol intake and lung function, adjusting for demographic and clinical covariates. Experimental data from animal and cell studies were analyzed using GraphPad Prism 10 and are presented as mean ± SD. Group comparisons were performed using Student's t-test or ANOVA (followed by Tukey's post hoc test) for normally distributed data, and Mann-Whitney U or Kruskal-Wallis tests for non-normal data, with $P < 0.05$ considered statistically significant. Detailed statistical analysis methods are described in Supplementary Method 2.9.

Journal Pre-proof

3. Results

3.1 Transcriptomics reveals shared oxidative stress and endothelial dysfunction in MV and CLP models

To investigate the mechanisms underlying these population-level associations, we first analyzed global transcriptomic changes in the MV- and CLP-induced lung injury models. When compared to controls, DEG analysis revealed that 86.8% of MV-upregulated genes and 87.2% of MV-downregulated genes were consistently altered in the CLP group, indicating strong transcriptional overlap (Fig 2A-B). This indicates overlapping gene regulatory mechanisms between the two interventions.

Heatmap analysis of the top 15 upregulated and downregulated genes in the MV group revealed highly concordant expression patterns in CLP, with strong reproducibility across biological replicates, supporting the robustness of these transcriptional changes (Fig 2C). GSEA based on DEGs in the MV group indicated a significant increase in ROS signaling pathway activity (NES = 2.04, Adjusted $P < 0.001$), suggesting oxidative stress as a core response mechanism (Fig 2D). Gene Ontology (GO) enrichment analysis further showed significant enrichment of differential genes in oxidative stress response pathways and endothelial function regulation pathways (Fig 2E). Notably, GSEA and GO analysis results for the CLP group exhibited highly similar enrichment profiles (Fig 2F-G), indicating that the two models share common molecular mechanisms in terms of oxidative stress and endothelial homeostasis disruption.

3.2 Single-cell RNA sequencing reveals impaired endothelial function and elevated oxidative stress in MV and CLP-driven lung injury

Building on the transcriptomic overlap identified in microarray, we turned to scRNA-seq to delineate cell-specific responses. We first analyzed self-sequenced high MV (H-MV) single-cell dataset. Lung tissues from 3 control mice and 3 H-MV-treated mice were dissociated into single-cell suspensions and subjected to scRNA-seq analysis. After rigorous quality control procedures, we retained 36,719 cells for downstream analysis, including 17,876 cells from control lungs and 18,843 cells from H-MV-treated lungs (Fig. 3A). Using UMAP for dimensionality reduction, we identified major lung-resident immune and structural cell populations, including Neutrophils (n = 4,999), Alveolar macrophages (n = 3,216), Interstitial macrophages (n = 676), Monocytes / Macrophages (n = 1,655), Dendritic cells (DCs) (n = 1,076), Basophils (n = 70), T cells (n = 4,047), B cells (n = 8,903), Natural killer cells (NK cells) (n = 1,275), Alveolar type I cells (AT1) (n = 260), Alveolar type II cells (AT2) (n = 1,701), Ciliated cells / Club cells (n = 107), Endothelial cells (n = 3,413), Mesothelial cells (n=53), Fibroblasts (n = 4,147), Myofibroblasts (n = 631), Smooth muscle cells (SMC) (n = 432), Megakaryocytes (n = 58) (Fig. 3B). For the CLP-induced lung injury-related dataset GSE207651 (Fig. 3C), after quality assessment and filtering, we retained transcriptomic data from 17,090 cells, with 7,103 cells derived from sham mouse lung tissue and 9,987 cells from CLP-treated mouse lung tissue. Using the same UMAP dimensionality reduction approach, we identified 30 cell clusters, which were classified into 14 major cell types (Fig. 3D). Neutrophils (n = 2,205), Alveolar macrophages (n = 833), Interstitial macrophages (n = 404), Monocytes (n = 1787), T cells (n = 1,179), B cells (n = 227), NK cells (n = 634), AT1 / Ciliated cells / Club cells (n = 233), AT2 (n = 179), Endothelial cells (n = 2,112), Mesothelial cells (n = 355), Fibroblasts (n = 5,764), Myofibroblasts (n = 263), SMC (n = 915). Further profiling of cellular composition changes in H-MV- and CLP-treated lung tissues demonstrated consistent trends—a pronounced increase in neutrophil infiltration coupled with a sharp reduction in endothelial cell abundance (Fig. 3E-F). Given the critical role of endothelial cells in maintaining endothelial

barrier integrity, we obtained a ROS-related gene set and conducted oxidative stress scoring specifically for endothelial cells. The results showed that oxidative stress levels were significantly increased in the lung endothelial cells of mice treated with H-MV and CLP (Fig. 3G-H). These findings strongly suggest that oxidative stress is likely a key factor mediating endothelial barrier injury induced by both mechanical stimulation and infection.

3.3 Associations between dietary intake of kaempferol and human lung functions

Kaempferol, as an antioxidant and active ingredient of Traditional Chinese Medicine, participates in a variety of biological functions and disease processes[48-50]. Some foods with high levels of kaempferol are shown in Figure S1. Considering these established pharmacological effects, our primary objective was to assess the potential relationship between regular dietary kaempferol consumption and lung function parameters at the population level.

Table S1 shows the baseline characteristics of adults stratified by dietary kaempferol intake quartiles (Q1-Q4) in NHANES from 2007 to 2010. Significant trends were observed across quartiles: age increased progressively from Q1 (42.03 ± 14.50 years) to Q4 (43.65 ± 13.68 years; $p = 0.002$). Sex distribution varied markedly, with Q4 showing the highest proportion of males (58%) and lowest of females (42%; $p < 0.001$). Racial composition shifted toward Non-Hispanic White dominance in higher quartiles (Q4: 76%), while Mexican American and Hispanic/Other groups declined ($p < 0.001$). Educational attainment rose across quartiles, with 64% in Q4 achieving college-level education ($p = 0.002$). Alcohol consumption increased sharply, from 72% non-drinkers in Q1 to 86% drinkers in Q4 ($p < 0.001$), though smoking prevalence showed no clear pattern ($p = 0.003$ for group differences

but no linear trend). Anthropometric trends included increased height from Q1 (167.46 ± 9.46 cm) to Q4 (171.40 ± 9.45 cm; $p < 0.001$), while BMI remained stable ($p = 0.611$). Blood biomarkers demonstrated upward trends: UA (uric acid), Albumin, and Bilirubin levels increased significantly across quartiles ($p < 0.001$ to $p = 0.035$), with HDL-C rising marginally (Q1: 51.08 ± 16.04 mg/dL to Q4: 53.41 ± 16.70 mg/dL; $p = 0.028$). Pulmonary function improved with higher quartiles, as evidenced by increased FVC, FEV1, and FEV1/FVC ratios (Except for the FEV1/FVC ratio $p = 0.002$, all p values are < 0.001). Notably, PRISm prevalence decreased from 47% in Q1 to 34% in Q4 ($p < 0.001$), suggesting an inverse association between the quartile metric and PRISm risk. Hyperlipidemia remained highly prevalent (~72%) across all groups ($p = 0.922$), with no significant differences in hypertension or diabetes prevalence.

FVC, FEV1, and PRISm were used as indicators reflecting impaired lung function[51, 52]. We examined the association between the dietary kaempferol and lung functions using the NHANES database. Based on the quartiles of dietary kaempferol intake, we divided all participants into four groups and systematically evaluated the intrinsic association between kaempferol intake and FVC. In unadjusted analyses (Model 1), continuous kaempferol intake showed significant positive associations with FVC. This association remained significant across increasing intake quartiles, particularly in Q4. After sequential adjustment for demographic factors (Model 2: age, sex, race, education, FPIR) and lifestyle/clinical covariates (Model 3: BMI, smoking, alcohol use, hypertension, diabetes, hyperlipidemia), both continuous intake and Q4 quartile associations maintained statistical significance. Given the well-documented gender disparities in dietary patterns and susceptibility to pulmonary diseases, we conducted stratified analyses by sex to explore potential differences in the association between kaempferol intake and FVC. This approach allowed us to examine whether the observed relationships varied between males and females. Notably, across all models, both

continuous kaempferol intake and its highest quartile (Q4) demonstrated a robust positive association with FVC in males, whereas no significant relationship was observed in females (Fig. 4A).

To further elucidate kaempferol's role in pulmonary function, we assessed its associations with FEV1 and PRISm separately. Kaempferol intake (continuous and Q4 quartile) was positively associated with FEV1 and negatively associated with PRISm in males, but not in females (Fig. 4B-C). Collectively, these findings indicate that kaempferol may exert a protective effect on pulmonary function in males.

3.4 Kaempferol targets ROS-producing NADPH oxidase

Using Ingenuity Pathway Analysis (IPA), we analyzed the top 30 potential molecular targets of kaempferol and identified NOX as one of the proteins directly regulated by the compound (Fig. 5A). We have proved that NOX family is one of the predominant sources of ROS in VILI[8], endothelial dysfunctions and vascular diseases[13-17, 53-55]. Subcellular localization analysis of the top 30 molecules targeted by kaempferol revealed that four are localized to the plasma membrane. Among these, only NOX is directly regulated by kaempferol, as indicated by the blue arrows (Fig. 5B).

In addition to acting as an antioxidant, we also explored whether kaempferol could interact directly with NOX2. The structure of NOX2 (Fig. 6A-D) was acquired from the Protein Data Bank (PDB) and the AlphaFold Protein Structure Database. The molecular structure of kaempferol (Fig. 6E) was retrieved from PubChem. To ensure a robust and comprehensive evaluation, we performed molecular docking using two representative cryo-EM structures: 7U8G[56] (Fig. 6A) and 8WEJ[57] (Fig. 6B). The 7U8G structure represents the heterodimeric core complex, consisting of the catalytic gp91^{phox} and p22^{phox}

subunits bound to the selective anti-NOX2-Fab 7G5. This model provides a high-resolution architectural foundation of the transmembrane catalytic core, capturing essential cofactors such as heme (HEM) and stabilizing membrane lipids (POV). In parallel, we utilized the 8WEJ structure, which represents an activated state. This assembly reflects a near-native functional state, comprising the $gp91^{phox}$-$p22^{phox}$ heterodimer with cytosolic activators $p47^{phox}$, $p67^{phox}$, and Rac1, along with the anti-NOX2-Fab 7D5. In addition, 8WEJ retains a comprehensive set of electron-transfer cofactors, including flavin adenine dinucleotide (FAD), a NADPH analogue (NDP), and HEM. We first utilized both the catalytic core (7U8G) and the active assembly (8WEJ) as docking receptors. The top two docking poses for the 7U8G-kaempferol interaction are presented in Fig. 6F-G. For the 8WEJ-kaempferol complex, the top two scores-selected (after filtering out orientations overlapping with the antibody fragment) are shown in Fig. 6H-I. Consistently high docking scores across both models provide compelling evidence for the binding plausibility of kaempferol to NOX2 and its potential to modulate enzymatic activity.

To ensure the robustness of our findings across different structural platforms, we extended our docking studies to protein models predicted by the AlphaFold Protein Structure Database. The structure here includes two versions of Alphafold DB v4 (Fig. 6C) and v6 (Fig. 6D). For each model, the two top-ranked poses are shown (Fig. 6J-M). The remaining docking results are shown in Fig S2-5.

Collectively, these docking analyses suggest that kaempferol may interact with multiple components of the NOX2 complex and thereby potentially influence NOX2 activation and ROS generation. In addition, NCF1 and DAPK1 shown in the IPA results can directly bind to kaempferol. We also performed molecular docking with kaempferol using these two molecular structures in the Alphafold database, and the results are shown in Fig. S6.

3.5 Mechanical ventilation promotes ROS generation and endothelial dysfunction in various lung regions

In the previous work, a mouse model of VILI was established using two ventilation strategies: low MV (L-MV) and H-MV[8]. The left lung was fixed in 4% paraformaldehyde and then embedded in paraffin for histological analysis, while the right upper lung lobe was embedded in optimal cutting temperature (OCT) compound, rapidly frozen in liquid nitrogen, and sectioned into 5 μm slices for dihydroethidium (DHE) staining or immunofluorescence staining[8]. The remaining lung lobes were frozen at -80°C for Western blot analysis[8]. Here, we established the same VILI model (Fig. 7A) while used the same lobe of the lung to explore the consistency of ROS generation and endothelial dysfunction in various lung regions. ROS levels were assessed using dihydroethidium (DHE) staining, lung tissues from ventilated mice exhibited stronger red fluorescent signal from oxidized DHE compared to the control group (Fig. 7B-C). Consistent with the DHE staining, total superoxide production in lung tissues was quantified by electron spin resonance (ESR) spectroscopy. Compared to the control group, ventilated mice in the L-MV and H-MV groups showed higher superoxide levels (Fig. 7D). Notably, the H-MV group exhibited the highest superoxide signal, confirming that increased tidal volumes significantly exacerbate oxidative stress in the lungs. The GSEA results demonstrated marked alterations in pathways associated with endothelial cell differentiation (Fig. 7E) and development (Fig. 7F) post-MV, suggesting impaired endothelial function. We used the same part (right upper lung lobe) to detect ROS production and the expression of endothelial junction proteins ZO-1, VE-cadherin, and Occludin after MV. Western blot analysis demonstrated a significant reduction of ZO-1, VE-cadherin, and Occludin in both ventilated groups compared to controls, suggesting MV induces the

disruption of the pulmonary endothelial barrier with more pronounced impairment observed in the H-MV group (Fig. 7G-H). Immunofluorescence staining also confirmed the downregulation of these three molecules under H-MV conditions (Fig. 7I-J). Linear correlation between ROS production and endothelial junction proteins was calculated. DHE fluorescence intensity was negatively correlated with the expression of ZO-1 ($r = -0.7041$, $P = 0.0034$), VE-cadherin ($r = -0.6322$, $P = 0.0115$), and Occludin ($r = -0.6877$, $P = 0.0046$) (Fig. 7K-M). Of note, these results were consistent in the different part of the same tissue as we previously examined[8] and in the same part of the same lung tissue as we proved here (Fig. 7N).

Therefore, MV promotes ROS generation and endothelial dysfunction in various lung regions. It's feasible to use different lobes in the same lung for exploration, which is more conducive to meeting the objective reality that it is difficult to obtain the same part of clinical samples.

3.6 Kaempferol alleviates endothelial dysfunction in mice with VILI via modulating NOX2/CaMKII/ERK1/2 signaling pathway

To investigate whether kaempferol can alleviate ROS-induced endothelial dysfunction in vivo, we pretreated mice with kaempferol prior to mice with H-MV. Western blot analysis revealed that the expression of NOX2 was significantly decreased (Fig. 8A-B) while the levels of ZO-1, VE-cadherin, and Occludin were significantly increased following kaempferol treatment (Fig. 8C-D).

Besides, we also detected the phosphorylation status of CaMKII and ERK1/2 in lung tissues following MV and MV+ kaempferol respectively. H-MV markedly increased the phosphorylation of CaMKII and ERK1/2, whereas kaempferol treatment significantly suppressed these effects, suggesting that kaempferol

effectively blocks ROS-mediated signal transduction in vivo (Fig. 8E-F).

3.7 Kaempferol preserves endothelial integrity under conditions of high cyclic stretch and oxidative stress in vitro

To determine whether kaempferol directly protects against high cyclic stretch- and ROS-induced endothelial barrier disruption in vitro, we treated HAECs with high cyclic stretch or H_2O_2, respectively. The 20%-0.5 Hz cyclic stretch was applied to HAECs in vitro using the Flexcell-5000 system (Fig. 9A) to simulate the rhythmic deformation induced by MV in vivo. Notably, kaempferol treatment effectively prevented the reduction in ZO-1 and VE-cadherin expression caused by either mechanical stress (high cyclic stretch; Fig. 9B-C) or oxidative stress (H_2O_2 exposure; Fig. 9D-E). DHE staining revealed that kaempferol markedly attenuated the H_2O_2-induced intracellular ROS elevation in HAECs (Fig. 9F-G). Consistently, ESR spectroscopy showed that H_2O_2 exposure significantly increased total superoxide production in HAECs, whereas kaempferol treatment effectively suppressed this elevation (Fig. 9H).

Collectively, these findings demonstrate that kaempferol preserves endothelial integrity under both mechanical and oxidative stress conditions in vitro.

3.8 Kaempferol ameliorates infection-induced lung injury through alleviating oxidative stress-caused endothelial dysfunction

In addition to investigating kaempferol's role in VILI, we also examined its therapeutic potential in infection-induced lung injury. Notably, pretreatment with kaempferol significantly enhanced survival rates in CLP model (Fig. 10A). Mirroring its suppression of pulmonary edema, kaempferol potently restored

endothelial barrier integrity, reversing the pronounced CLP-triggered Evans Blue leakage (Fig. 10B). Compared to the sham group, the CLP group exhibited a marked elevation in lung wet-to-dry weight ratio, which was substantially attenuated by kaempferol administration (Fig. 10C). Histopathological analysis revealed that kaempferol markedly attenuated vascular leakage, hemorrhage, inflammatory cell infiltration, and alveolar wall thickening, resulting in a significantly lower lung injury score (Fig. 10D-E).

Kaempferol treatment significantly reduced NOX2 expression in the CLP model (Fig. 10F-G). While CLP markedly downregulated endothelial junction proteins (ZO-1 and VE-cadherin), kaempferol restored their expression (Fig. 10H-I). Furthermore, kaempferol suppressed CLP-induced activation of the ROS/CaMKII/ERK1/2 pathway (Fig. 10J-K).

Collectively, kaempferol not only prevents VILI but also exerts stronger protective effects against infection-driven lung injury.

Journal Pre-proof

Journal Pre-proof

4. Discussion

Mechanical ventilation remains indispensable in critical care, but the harmful mechanical stress generated during ventilation could induce VILI. By integrating epidemiological observations, transcriptomic profiling, single-cell analyses, and mechanistic studies, we provide compelling evidence that ROS serves as a central driver of endothelial barrier disruption across diverse forms of lung injury, Notably, we further show for the first time that VILI is characterized by a marked increase of oxidative stress in various part of the lung. Consistent with these observations, we identify oxidative stress-driven endothelial dysfunction as a unifying pathogenic mechanism shared by both VILI and CLP-associated acute lung injury. Within this framework, kaempferol emerged as a candidate intervention that acts at the source of ROS, thereby preserving endothelial barrier integrity and mitigating downstream tissue damage.

Numerous flavonoid compounds have been shown to possess anti-inflammatory and antioxidant properties, among which kaempferol has attracted particular attention due to its broad spectrum of biological activities[58, 59]. Previous studies have demonstrated the protective effects of kaempferol in various pulmonary diseases, including lung ischemia–reperfusion injury[60], LPS- and CLP-induced acute lung injury[61, 62], and non-small cell lung cancer (NSCLC)[63]. ~~However, whether kaempferol exerts a protective role in VILI under abnormal cyclic stretch remains unclear. Its potential to ameliorate VILI-associated endothelial dysfunction and its therapeutic effects on pre-existing pulmonary injury require further investigation.~~ Previous studies have reported associations between dietary flavonoid intake and respiratory health outcomes[64, 65]. In our epidemiological analysis, dietary kaempferol intake was positively correlated with lung function in male subjects. This male-specific signaling motivated us to conduct subsequent mechanistic validation in male mice. The NOX family represents a major enzymatic source of ROS and is widely activated in various lung injury models and vascular

diseases[12, 13, 53, 66-68]. Different NOX isoforms exhibit cell-specific roles in distinct vascular pathologies[12]. We have proved that endothelial NOX2-induced ROS promotes endothelial dysfunction and lung injury under high cyclic stretch subjected to MV[8]. Therefore, inhibiting NOX2 and targeting ROS are potential therapeutic strategies for treating lung injury. This study proved that kaempferol mitigates VILI and pre-existing pulmonary damage by modulating MV-generated ROS, with a focus on the role of NOX2 in this mechanism.

Previous studies have shown that antioxidant or redox-modulating interventions, including 4-octyl itaconate[20], amifostine[21], superoxide dismutase[22], and N-acetylcysteine[23], can alleviate experimental ventilator-induced lung injury, supporting oxidative stress as a therapeutically relevant target in VILI. However, most of these studies mainly focused on isolated VILI model and did not address whether VILI and infection-associated lung injury share a common endothelial oxidative stress program. Here, we reveal a shared pathogenic pathway in MV- and sepsis-induced lung injury, driven by persistent oxidative stress and resulting in widespread endothelial dysfunction. Additionally, our study incorporates an extensive epidemiological analysis demonstrating an association between kaempferol and enhanced lung function, further substantiating its potential as a therapeutic agent in lung injury.

Regarding the sex-specific association between dietary kaempferol intake and lung function, we speculate that sex hormones may be a major driver of this heterogeneity. Under physiological conditions, females appear less susceptible to oxidative stress, potentially due to the antioxidative properties of estrogen and sex-dependent regulation of NOX activity[69]. In healthy young adults, in vivo oxidative stress biomarkers were reported to be significantly higher in men than in age-matched women[70]. From the perspective of ROS generation, sex differences may exist at the level of NOX isoform expression and activation[71]. For example, NOX2 expression was reported to be higher in

isolated porcine coronary arteries from males, whereas females showed relatively higher NOX4 expression[72]. However, other work reported no significant sex difference in NOX2 expression in rat cerebral arteries, with sex-related effects observed primarily for NOX1 and NOX4[73], Although the existing literature does not provide consistent evidence that NOX2 expression is higher in males than in females, these findings collectively suggest that sex-dependent differences in NOX expression or activity may modulate the therapeutic effects of kaempferol. Estrogen levels also modulate ROS clearance, which may further contribute to sex-related differences in overall ROS level. Higher levels of estrogen are associated with increased expression of extracellular superoxide dismutase (ecSOD) and manganese superoxide dismutase (MnSOD) in circulating monocytes, which may contribute to the clearance of ROS and partially mediate the vascular protective effect of estrogen[74].

Given the central role of endothelial barrier integrity in gas exchange, preserving the alveolar–capillary endothelium represents a rational therapeutic objective in VILI. In the mammalian lung, alveolar and capillary ECs form a tightly integrated structural barrier essential for efficient gas exchange[75]. MV with non-physiological parameters induces direct mechanical injury to these ECs, compromising barrier integrity[5]. Therefore, pharmacological interventions preserving endothelial integrity may offer a promising therapeutic avenue for VILI management. To date, studies on endothelial mechanotransduction in VILI have largely explored the role of mechanosensitive receptors, particularly ion channels and integrins, in disease pathogenesis[76-78]. However, the role of mechanical stress and infection-induced ROS in endothelial dysfunction and lung injury was not clarified clearly. Here, we demonstrate for the first time that kaempferol attenuates NOX2-driven ROS production, thereby alleviating endothelial dysfunction and lung injury by suppressing the CaMKII-ERK1/2 signaling pathway under high cyclic stretch. Notably, mechanical cues—including stretch, stiffness, circadian rhythms, fluid flow, intercellular

signaling cascades, and cytoskeletal organization—can modulate drug-target interactions, offering critical insights for drug discovery and development[79]. This aspect remains underexplored in the current study, and future research should incorporate it to provide a more comprehensive understanding.

Several limitations of the present study should be acknowledged. First, kaempferol is a well-recognized flavonol with intrinsic antioxidant and ROS-scavenging properties. Therefore, we cannot exclude the possibility that at least part of its protective effects in our VILI and CLP models results from its general antioxidant activity rather than direct inhibition of NOX2. While molecular docking suggests a potential interaction between kaempferol and NOX2, these findings remain computational and lack direct experimental validation of NOX2 enzymatic inhibition. Second, our in vivo experiments employed a pretreatment design, which does not fully recapitulate the clinical scenario where mechanical ventilation is initiated emergently. Future studies should explore post-injury therapeutic dosing to establish an effective treatment window.

Collectively, kaempferol exerts robust protection in both VILI and CLP-induced lung injury, primarily via inhibition of NOX2-derived oxidative stress and associated signaling pathways. These data not only validate oxidative stress as a key driver of endothelial dysfunction but also position kaempferol as a promising candidate for treating pulmonary disorders involving redox imbalance in man.

Journal Pre-proof

AUTHOR CONTRIBUTIONS

Z. S.: Methodology, Investigation, Formal analysis, Visualization, Data curation, Writing-original draft preparation. Z. G.: Methodology, Investigation, Formal analysis, Data curation, Visualization, Writing-original draft preparation. W. T.: Methodology, Visualization, Writing-review & Editing. F. Z.: Methodology, Investigation, Formal analysis, Data-processing, Visualization. T. J.: Methodology, Visualization. W. H.: Methodology, Visualization. Q. Y.: Methodology, Writing-review & Editing, Supervision. Y. H.: Methodology, Writing-review & Editing, Supervision. Y. Q.: Methodology, Writing-review & Editing, Supervision, Funding acquisition. H. W.: Methodology, Formal analysis, Writing-review & Editing, Supervision, Project administration. K. H.: Conceptualization, Investigation, Formal analysis, Visualization, Data curation, Writing-original draft preparation, Writing-review & Editing, Supervision, Project administration, Funding acquisition.

ACKNOWLEDGMENTS

This research was supported by grants from the National Natural Science Foundation of China (grant numbers 12032003 and 12302409), Shanghai Jiao Tong University Medical-Engineering Interdisciplinary Research Fund (YG2025QNB36) and The Science and Technology Commission of Shanghai Municipality (23S31906100).

ETHICS STATEMENT

All procedures involving animals were approved by the Animal Ethics Committee of Shanghai Jiao Tong University and conducted in accordance with the Regulations for the Administration of Affairs Concerning Experimental Animals (Decree No. 55, 2001, Ministry of Health, China).

DECLARATION OF INTERESTS

The authors declare no competing interests.

1

Journal Pre-proof

REFERENCES

1. Walter K. Mechanical Ventilation. *JAMA*. 2021;326:1452. https://doi.org/10.1001/jama.2021.13084
2. Fogagnolo A, Montanaro F, Al-Husinat Li, Turrini C, Rauseo M, Mirabella L, Ragazzi R, Ottaviani I, Cinnella G, Volta CA and Spadaro S. Management of Intraoperative Mechanical Ventilation to Prevent Postoperative Complications after General Anesthesia: A Narrative Review. *Journal of clinical medicine*. 2021;10:2656. https://doi.org/10.3390/jcm10122656
3. Acute Respiratory Distress Syndrome N, Brower RG, Matthay MA, Morris A, Schoenfeld D, Thompson BT and Wheeler A. Ventilation with lower tidal volumes as compared with traditional tidal volumes for acute lung injury and the acute respiratory distress syndrome. *The New England journal of medicine*. 2000;342:1301-8. https://doi.org/10.1056/NEJM200005043421801
4. Banavasi H, Nguyen P, Osman H and Soubani AO. Management of ARDS - What Works and What Does Not. *The American journal of the medical sciences*. 2021;362:13-23. https://doi.org/10.1016/j.amjms.2020.12.019
5. Wang T, Gross C, Desai AA, Zemskov E, Wu X, Garcia AN, Jacobson JR, Yuan JXJ, Garcia JGN and Black SM. Endothelial cell signaling and ventilator-induced lung injury: molecular mechanisms, genomic analyses, and therapeutic targets. *American journal of physiology Lung cellular and molecular physiology*. 2017;312:L452-L476. https://doi.org/10.1152/ajplung.00231.2016
6. Matthay MA, Bhattacharya S, Gaver D, Ware LB, Lim LHK, Syrkina O, Eyal F and Hubmayr R. Ventilator-induced lung injury: in vivo and in vitro mechanisms. *American journal of physiology Lung cellular and molecular physiology*. 2002;283:L678-82. https://doi.org/10.1152/ajplung.00154.2002
7. Fan E, Brodie D and Slutsky AS. Acute Respiratory Distress Syndrome: Advances in Diagnosis and Treatment. *JAMA*. 2018;319:698-710. https://doi.org/10.1001/jama.2017.21907
8. Jiang T, Zhang Y, Guo Z, Ren H, Hu W, Yao Q, Huo Y, Qi Y and Huang K. Mechanical Stress Induced NOX2 Promotes Endothelial Dysfunction in Ventilator-Induced Lung Injury: Potential Treatment with Quercetin. *Advanced science (Weinheim, Baden-Wurttemberg, Germany)*. 2025;12:e2502639. https://doi.org/10.1002/advs.202502639
9. Gu Z, Sun M, Liu J, Huang Q, Wang Y, Liao J, Shu T, Tao M, Mao G, Pei Z, Meng W, Zhang X, Wei Y, Zhang S, Li S, Xiao K, Lu Y and Xu Q. Endothelium-Derived Engineered Extracellular Vesicles Protect the Pulmonary Endothelial Barrier in Acute Lung Injury. *Advanced science (Weinheim, Baden-Wurttemberg, Germany)*. 2024;11:e2306156. https://doi.org/10.1002/advs.202306156
10. Hong H, Wu Y, Li Y, Han Y, Cao X, Wu VWY, Chan TTH, Zhou J, Cao Q, Lui KO, Wong C-K, Dai Z and Tian XY. Endothelial PPARδ Ablation Exacerbates Vascular Hyperpermeability via STAT1/CXCL10 Signaling in Acute Lung Injury. *Circulation research*. 2025;136:735-751. https://doi.org/10.1161/CIRCRESAHA.124.325855
11. Khan N, Kumar V, Li P, Group RS, Schlapbach LJ, Boyd AW, Coulthard MG and Woodruff TM. Inhibiting Eph/ephrin signaling reduces vascular leak and endothelial cell dysfunction in mice with sepsis. *Science translational medicine*. 2024;16:eadg5768. https://doi.org/10.1126/scitranslmed.adg5768
12. Zhang Y, Murugesan P, Huang K and Cai H. NADPH oxidases and oxidase crosstalk in cardiovascular diseases: novel therapeutic targets. *Nat Rev Cardiol*. 2020;17:170-194. https://doi.org/10.1038/s41569-019-0260-8

13. Jiang J, Huang K, Xu S, Garcia JGN, Wang C and Cai H. Targeting NOX4 alleviates sepsis-induced acute lung injury via attenuation of redox-sensitive activation of CaMKII/ERK1/2/MLCK and endothelial cell barrier dysfunction. *Redox Biol*. 2020;36:101638. https://doi.org/10.1016/j.redox.2020.101638

14. Huang K, Wang Y, Siu KL, Zhang Y and Cai H. Targeting feed-forward signaling of TGFβ/NOX4/DHFR/eNOS uncoupling/TGF β axis with anti-TGFβ and folic acid attenuates formation of aortic an eurysms: Novel mechanisms and therapeutics. *Redox biology*. 2021;38:101757. https://doi.org/10.1016/j.redox.2020.101757

15. Huang K, Narumi T, Zhang Y, Li Q, Murugesan P, Wu Y, Liu NM and Cai H. Targeting MicroRNA-192-5p, a Downstream Effector of NOXs (NADPH Oxidases), Reverses Endothelial DHFR (Dihydrofolate Reductase) Deficiency to Attenuate Abdominal Aortic Aneurysm Formation. *Hypertension (Dallas, Tex : 1979)*. 2021;78:282-293. https://doi.org/10.1161/HYPERTENSIONAHA.120.15070

16. Youn JY, Wang J, Li Q, Huang K and Cai H. Robust therapeutic effects on COVID-19 of novel small molecules: Alleviation of SARS-CoV-2 S protein induction of ACE2/TMPRSS2, NOX2/ROS, an d MCP-1. *Frontiers in cardiovascular medicine*. 2022;9:957340. https://doi.org/10.3389/fcvm.2022.957340

17. Ren H, Hu W, Jiang T, Yao Q, Qi Y and Huang K. Mechanical stress induced mitochondrial dysfunction in cardiovascular diseases: Novel mechanisms and therapeutic targets. *Biomedicine & pharmacotherapy = Biomedecine & pharmacotherapie*. 2024;174:116545. https://doi.org/10.1016/j.biopha.2024.116545

18. Birukov KG. Cyclic stretch, reactive oxygen species, and vascular remodeling. *Antioxidants & redox signaling*. 2009;11:1651-67. https://doi.org/10.1089/ars.2008.2390

19. Paravicini TM and Touyz RM. Redox signaling in hypertension. *Cardiovascular research*. 2006;71:247-58. https://doi.org/10.1016/j.cardiores.2006.05.001

20. Wang X, Kong W, Yang R and Yang C. 4-octyl itaconate ameliorates ventilator-induced lung injury. *Arch Biochem Biophys*. 2024;752:109853. https://doi.org/10.1016/j.abb.2023.109853

21. Fu P, Murley JS, Grdina DJ, Birukova AA and Birukov KG. Induction of cellular antioxidant defense by amifostine improves ventilator-induced lung injury. *Crit Care Med*. 2011;39:2711-21. https://doi.org/10.1097/CCM.0b013e3182284a5f

22. Wu N-C, Liao F-T, Cheng H-M, Sung S-H, Yang Y-C and Wang J, Jr. Intravenous superoxide dismutase as a protective agent to prevent impairment of lung function induced by high tidal volume ventilation. *BMC Pulm Med*. 2017;17:105. https://doi.org/10.1186/s12890-017-0448-9

23. Chiang C-H, Chuang C-H, Liu S-L, Chian C-F, Zhang H and Ryu JH. N-acetylcysteine attenuates ventilator-induced lung injury in an isolated and perfused rat lung model. *Injury*. 2012;43:1257-63. https://doi.org/10.1016/j.injury.2011.12.026

24. Devi KP, Malar DS, Nabavi SF, Sureda A, Xiao J, Nabavi SM and Daglia M. Kaempferol and inflammation: From chemistry to medicine. *Pharmacological research*. 2015;99:1-10. https://doi.org/10.1016/j.phrs.2015.05.002

25. Calderon-Montano JM, Burgos-Moron E, Perez-Guerrero C and Lopez-Lazaro M. A review on the dietary flavonoid kaempferol. *Mini Rev Med Chem*. 2011;11:298-344. https://doi.org/10.2174/138955711795305335

26. Chen M, Zhao E, Li M, Xu M, Hao S, Gao Y, Wu X, Li X, Yu Y, Yu Z and Yin Y. Kaempferol inhibits non-homologous end joining repair via regulating Ku80 stability in glioma cancer. *Phytomedicine*. 2023;116:154876. https://doi.org/10.1016/j.phymed.2023.154876

27. Xu H, Yu S, Lin C, Dong D, Xiao J, Ye Y and Wang M. Roles of flavonoids in ischemic heart disease: Cardioprotective effects and mechanisms against myocardial ischemia and reperfusion injury. *Phytomedicine*. 2024;126:155409. https://doi.org/10.1016/j.phymed.2024.155409

28. Wan ES, Balte P, Schwartz JE, Bhatt SP, Cassano PA, Couper D, Daviglus ML, Dransfield MT, Gharib SA, Jacobs DR, Jr., Kalhan R, London SJ, Navas-Acien A, O'Connor GT, Sanders JL, Smith BM, White W, Yende S and Oelsner EC. Association Between Preserved Ratio Impaired Spirometry and Clinical Outcomes in US Adults. *JAMA*. 2021;326:2287-2298. https://doi.org/10.1001/jama.2021.20939

29. Basil MC, Cardenas-Diaz FL, Kathiriya JJ, Morley MP, Carl J, Brumwell AN, Katzen J, Slovik KJ, Babu A, Zhou S, Kremp MM, McCauley KB, Li S, Planer JD, Hussain SS, Liu X, Windmueller R, Ying Y, Stewart KM, Oyster M, Christie JD, Diamond JM, Engelhardt JF, Cantu E, Rowe SM, Kotton DN, Chapman HA and Morrisey EE. Human distal airways contain a multipotent secretory cell that can regenerate alveoli. *Nature*. 2022;604:120-126. https://doi.org/10.1038/s41586-022-04552-0

30. Bian F, Lan Y-W, Zhao S, Deng Z, Shukla S, Acharya A, Donovan J, Le T, Milewski D, Bacchetta M, Hozain AE, Tipograf Y, Chen Y-W, Xu Y, Shi D, Kalinichenko VV and Kalin TV. Lung endothelial cells regulate pulmonary fibrosis through FOXF1/R-Ras signaling. *Nature communications*. 2023;14:2560. https://doi.org/10.1038/s41467-023-38177-2

31. Han S, Lee M, Shin Y, Giovanni R, Chakrabarty RP, Herrerias MM, Dada LA, Flozak AS, Reyfman PA, Khuder B, Reczek CR, Gao L, Lopéz-Barneo J, Gottardi CJ, Budinger GRS and Chandel NS. Mitochondrial integrated stress response controls lung epithelial cell fate. *Nature*. 2023;620:890-897. https://doi.org/10.1038/s41586-023-06423-8

32. Muendlein HI, Connolly WM, Cameron J, Jetton D, Magri Z, Smirnova I, Vannier E, Li X, Martinot AJ, Batorsky R and Poltorak A. Neutrophils and macrophages drive TNF-induced lethality via TRIF/CD14- mediated responses. *Science immunology*. 2022;7:eadd0665. https://doi.org/10.1126/sciimmunol.add0665

33. Rodor J, Chen SH, Scanlon JP, Monteiro JP, Caudrillier A, Sweta S, Stewart KR, Shmakova A, Dobie R, Henderson BEP, Stewart K, Hadoke PWF, Southwood M, Moore SD, Upton PD, Morrell NW, Li Z, Chan SY, Handen A, Lafyatis R, de Rooij LPMH, Henderson NC, Carmeliet P, Spiroski AM, Brittan M and Baker AH. Single-cell RNA sequencing profiling of mouse endothelial cells in response to pulmonary arterial hypertension. *Cardiovascular research*. 2022;118:2519-2534. https://doi.org/10.1093/cvr/cvab296

34. Schupp JC, Adams TS, Cosme C, Jr., Raredon MSB, Yuan Y, Omote N, Poli S, Chioccioli M, Rose K-A, Manning EP, Sauler M, DeIuliis G, Ahangari F, Neumark N, Habermann AC, Gutierrez AJ, Bui LT, Lafyatis R, Pierce RW, Meyer KB, Nawijn MC, Teichmann SA, Banovich NE, Kropski JA, Niklason LE, Pe'er D, Yan X, Homer RJ, Rosas IO and Kaminski N. Integrated Single-Cell Atlas of Endothelial Cells of the Human Lung. *Circulation*. 2021;144:286-302. https://doi.org/10.1161/CIRCULATIONAHA.120.052318

35. Kumar R, Nolan K, Kassa B, Chanana N, Palmo T, Sharma K, Singh K, Mickael C, Fonseca Balladares D, Nilsson J, Prabhakar A, Mishra A, Lee MH, Sanders L, Kumar S, Molofsky AB, Stenmark KR, Sheppard D, Tuder RM, Gupta MD, Thinlas T, Pasha Q and Graham BB. Monocytes and interstitial macrophages contribute to hypoxic pulmonary hypertension. *The Journal of clinical investigation*. 2025;135:e176865. https://doi.org/10.1172/JCI176865

36. Bowerman C, Bhakta NR, Brazzale D, Cooper BR, Cooper J, Gochicoa-Rangel L, Haynes J, Kaminsky DA, Lan LTT, Masekela R, McCormack MC, Steenbruggen I and Stanojevic S. A Race-neutral Approach to the Interpretation of Lung Function Measure ments. *American journal of respiratory and critical care medicine*. 2023;207:768-774. https://doi.org/10.1164/rccm.202205-0963OC

37. Zhang W, Zhou Q, Yang W, Tan X, Xu Y and Yi Z. Relationship between dietary flavan-3-ols intake and mortality in metabolic syndrome population; a large cohort study. *Frontiers in nutrition*. 2025;12:1572189. https://doi.org/10.3389/fnut.2025.1572189

38. Huang K, Bao H, Yan Z-Q, Wang L, Zhang P, Yao Q-P, Shi Q, Chen X-H, Wang K-X, Shen B-R, Qi Y-X and Jiang Z-L. MicroRNA-33 protects against neointimal hyperplasia induced by arterial mechanical stretch in the grafted vein. *Cardiovascular research*. 2017;113:488-497. https://doi.org/10.1093/cvr/cvw257

39. Yang Y-C, Wang X-D, Huang K, Wang L, Jiang Z-L and Qi Y-X. Temporal phosphoproteomics to investigate the mechanotransduction of vascular smooth muscle cells in response to cyclic stretch. *Journal of biomechanics*. 2014;47:3622-9. https://doi.org/10.1016/j.jbiomech.2014.10.008

40. Huang K, Yan Z-Q, Zhao D, Chen S-G, Gao L-Z, Zhang P, Shen B-R, Han H-C, Qi Y-X and Jiang Z-L. SIRT1 and FOXO Mediate Contractile Differentiation of Vascular Smooth Muscle Cells under Cyclic Stretch. *Cell Physiol Biochem*. 2015;37:1817-29. https://doi.org/10.1159/000438544

41. Qi Y-X, Yao Q-P, Huang K, Shi Q, Zhang P, Wang G-L, Han Y, Bao H, Wang L, Li H-P, Shen B-R, Wang Y, Chien S and Jiang Z-L. Nuclear envelope proteins modulate proliferation of vascular smooth muscle cells during cyclic stretch application. *Proc Natl Acad Sci U S A*. 2016;113:5293-8. https://doi.org/10.1073/pnas.1604569113

42. Wang L, Bao H, Wang K-X, Zhang P, Yao Q-P, Chen X-H, Huang K, Qi Y-X and Jiang Z-L. Secreted miR-27a Induced by Cyclic Stretch Modulates the Proliferation of Endothelial Cells in Hypertension via GRK6. *Scientific reports*. 2017;7:41058. https://doi.org/10.1038/srep41058

43. Bao H, Li H-P, Shi Q, Huang K, Chen X-H, Chen Y-X, Han Y, Xiao Q, Yao Q-P and Qi Y-X. Lamin A/C negatively regulated by miR-124-3p modulates apoptosis of vascular smooth muscle cells during cyclic stretch application in rats. *Acta physiologica (Oxford, England)*. 2020;228:e13374. https://doi.org/10.1111/apha.13374

44. Yang Y, Qian B, Zhou D, Zhu F, Lei D, Huang S, Wang X, Ye X, Huang K, Yang Q and Zhao Q. External stent ameliorates vein graft remodeling through Ajuba-mediated suppression of Hippo signaling pathway. *Biomaterials advances*. 2025;177:214427. https://doi.org/10.1016/j.bioadv.2025.214427

45. Ma T, Tian W, Zhu F, Qi Y and Huang K. Injury and cyclic stretch induce vein graft failure: effective treatment with zinc oxide-loaded electrospun polycaprolactone external stent. *Regenerative biomaterials*. 2025;12:rbaf119. https://doi.org/10.1093/rb/rbaf119

46. Liu J, Chen K, Tang M, Mu Q, Zhang S, Li J, Liao J, Jiang X and Wang C. Oxidative stress and inflammation mediate the adverse effects of cadmium exposure on all-cause and cause-specific mortality in patients with diabetes and prediabetes. *Cardiovascular diabetology*. 2025;24:145. https://doi.org/10.1186/s12933-025-02698-5

47. Xu Z, Liu D, Zhai Y, Tang Y, Jiang L, Li L and Wu Q. Association between the oxidative balance score and all-cause and cardiovascular mortality in patients with diabetes and prediabetes. *Redox Biol*. 2024;76:103327. https://doi.org/10.1016/j.redox.2024.103327

48. Huang K, Zhang P, Zhang Z, Youn JY, Wang C, Zhang H and Cai H. Traditional Chinese Medicine (TCM) in the treatment of COVID-19 and other viral infections: Efficacies and mechanisms. *Pharmacology & therapeutics*. 2021;225:107843. https://doi.org/10.1016/j.pharmthera.2021.107843

49. Chen J, Zhong H, Huang Z, Chen X, You J and Zou T. A Critical Review of Kaempferol in Intestinal Health and Diseases. *Antioxidants (Basel, Switzerland)*. 2023;12:1642. https://doi.org/10.3390/antiox12081642

50. Chen H, Su X, Xiang P, Wei Y, Wang H, Li J, Liu S, Mei W and Dai H. Identification of Chemical Constituents from Leaves and Stems of Alpinia oxyphylla: Potential Antioxidant and Tyrosinase Inhibitory Properties. *Antioxidants (Basel, Switzerland)*. 2024;13:1538. https://doi.org/10.3390/antiox13121538

51. Yang S, Liao G and Tse LA. Association of preserved ratio impaired spirometry with mortality: a systematic review and meta-analysis. *European respiratory review : an official journal of the European Resp iratory Society*. 2023;32:230135. https://doi.org/10.1183/16000617.0135-2023

52. Chen C, Huang Z, Liu L, Su B, Feng Y and Huang Y. Lung Function Impairment and Risks of Incident Cardiovascular Diseases and Mortality Among People With Type 2 Diabetes: A Prospective Cohort Study. *Diabetes care*. 2025;48:728-736. https://doi.org/10.2337/dc24-2188

53. Zhang Y, Youn JY, Huang K, Zhang Y and Cai H. Alleviation of accelerated diabetic atherogenesis in STZ-treated apoE/NOX1 DKO mice, apoE(-/-)/tg-EC-DHFR mice, and by folic acid. *Redox Biol*. 2025;82:103570. https://doi.org/10.1016/j.redox.2025.103570

54. Zong NC, Huang K, Yang X and Cai H. Expand the success of screening to reduce aortic aneurysm mortality: progress interpretation and new fronts. *Trends in cardiovascular medicine*. 2025;35:221-229. https://doi.org/10.1016/j.tcm.2024.12.004

55. Huang K, Wu Y, Zhang Y, Youn JY and Cai H. Combination of folic acid with nifedipine is completely effective in a ttenuating aortic aneurysm formation as a novel oral medication. *Redox Biol*. 2022;58:102521. https://doi.org/10.1016/j.redox.2022.102521

56. Noreng S, Ota N, Sun Y, Ho H, Johnson M, Arthur CP, Schneider K, Lehoux I, Davies CW, Mortara K, Wong K, Seshasayee D, Masureel M, Payandeh J, Yi T and Koerber JT. Structure of the core human NADPH oxidase NOX2. *Nature communications*. 2022;13:6079. https://doi.org/10.1038/s41467-022-33711-0

57. Liu X, Shi Y, Liu R, Song K and Chen L. Structure of human phagocyte NADPH oxidase in the activated state. *Nature*. 2024;627:189-195. https://doi.org/10.1038/s41586-024-07056-1

58. Bangar SP, Chaudhary V, Sharma N, Bansal V, Ozogul F and Lorenzo JM. Kaempferol: A flavonoid with wider biological activities and its applications. *Crit Rev Food Sci Nutr*. 2023;63:9580-9604. https://doi.org/10.1080/10408398.2022.2067121

59. Guo Z, Liao Z, Huang L, Liu D, Yin D and He M. Kaempferol protects cardiomyocytes against anoxia/reoxygenation injury via mitochondrial pathway mediated by SIRT1. *Eur J Pharmacol*. 2015;761:245-53. https://doi.org/10.1016/j.ejphar.2015.05.056

60. Yang C, Yang W, He Z, Guo J, Yang X, Wang R and Li H. Kaempferol Alleviates Oxidative Stress and Apoptosis Through Mitochond ria-dependent Pathway During Lung Ischemia-Reperfusion Injury. *Frontiers in pharmacology*. 2021;12:624402. https://doi.org/10.3389/fphar.2021.624402

61. Gao M, Zhu X, Gao X, Yang H, Li H, Du Y, Gao J, Chen Z, Dong H, Wang B and Zhang L. Kaempferol mitigates sepsis-induced acute lung injury by modulating the SphK1/S1P/S1PR1/MLC2 signaling pathway to restore the integrity of the pulmonary endothelial cell barrier. *Chem Biol Interact*. 2024;398:111085. https://doi.org/10.1016/j.cbi.2024.111085

62. Wang B, Gu A, Yan J, Zhang Y, Liu J, Sun C, Wei Y, Gu C and Wang Y. Kaempferol alleviates sepsis related acute lung injury by inhibiting the activation of alveolar macrophages mediated by extracellular vesicles from alveolar epithelial cells. *Int Immunopharmacol*. 2025;162:115130. https://doi.org/10.1016/j.intimp.2025.115130

63. Zhang J, Liu X, Zhang G, Wu J, Liu Z, Liu C, Wang H, Miao S, Deng L, Cao K, Shang M, Zhu Q and Sun P. To explore the effect of kaempferol on non-small cell lung cancer based on network

pharmacology and molecular docking. *Front Pharmacol*. 2023;14:1148171. https://doi.org/10.3389/fphar.2023.1148171

64. Bondonno NP, Parmenter BH, Thompson AS, Jennings A, Murray K, Rasmussen DB, Tresserra-Rimbau A, Kühn T and Cassidy A. Flavonoid intakes, chronic obstructive pulmonary disease, adult asthma , and lung function: a cohort study in the UK Biobank. *The American journal of clinical nutrition*. 2024;120:1195-1206. https://doi.org/10.1016/j.ajcnut.2024.08.032

65. Sun M and Ding Q. Correlation of dietary flavonoid intake with chronic bronchitis, emphy sema, and asthma in U.S. adults: A large, national, cross-sectional st udy. *PloS one*. 2024;19:e0309310. https://doi.org/10.1371/journal.pone.0309310

66. Jiang T, Zhang Y, Guo Z, Ren H, Hu W, Yao Q, Huo Y, Qi Y and Huang K. Mechanical Stress Induced NOX2 Promotes Endothelial Dysfunction in Ventilator-Induced Lung Injury: Potential Treatment with Quercetin. *Adv Sci (Weinh)*. 2025;12:e2502639. https://doi.org/10.1002/advs.202502639

67. Sies H and Jones DP. Reactive oxygen species (ROS) as pleiotropic physiological signalling agents. *Nat Rev Mol Cell Biol*. 2020;21:363-383. https://doi.org/10.1038/s41580-020-0230-3

68. Ziqi S and Kai H. Cyclic stretch and oxidative stress induced miRNAs in vascular remodeling. *Biophysics Reports*. 2025;0:- %8. https://doi.org/10.52601/bpr.2025.250033 %U https://www.biophysics-reports.org/en/article/id/29c00be4-dcf9-4b22-9758-c8e366438861

69. Kander MC, Cui Y and Liu Z. Gender difference in oxidative stress: a new look at the mechanisms for cardiovascular diseases. *Journal of cellular and molecular medicine*. 2017;21:1024-1032. https://doi.org/10.1111/jcmm.13038

70. Ide T, Tsutsui H, Ohashi N, Hayashidani S, Suematsu N, Tsuchihashi M, Tamai H and Takeshita A. Greater oxidative stress in healthy young men compared with premenopausal women. *Arteriosclerosis, thrombosis, and vascular biology*. 2002;22:438-42. https://doi.org/10.1161/hq0302.104515

71. Miller AA, De Silva TM, Jackman KA and Sobey CG. Effect of gender and sex hormones on vascular oxidative stress. *Clinical and experimental pharmacology & physiology*. 2007;34:1037-43. https://doi.org/10.1111/j.1440-1681.2007.04732.x

72. Wong PS, Randall MD and Roberts RE. Sex differences in the role of NADPH oxidases in endothelium-dependent vasorelaxation in porcine isolated coronary arteries. *Vascular pharmacology*. 2015;72:83-92. https://doi.org/10.1016/j.vph.2015.04.001

73. Miller AA, Drummond GR, Mast AE, Schmidt HHHW and Sobey CG. Effect of gender on NADPH-oxidase activity, expression, and function in the cerebral circulation: role of estrogen. *Stroke*. 2007;38:2142-9. https://doi.org/10.1161/STROKEAHA.106.477406

74. Strehlow K, Rotter S, Wassmann S, Adam O, Grohé C, Laufs K, Böhm M and Nickenig G. Modulation of antioxidant enzyme expression and function by estrogen. *Circulation research*. 2003;93:170-7. https://doi.org/10.1161/01.RES.0000082334.17947.11

75. Gillich A, Zhang F, Farmer CG, Travaglini KJ, Tan SY, Gu M, Zhou B, Feinstein JA, Krasnow MA and Metzger RJ. Capillary cell-type specialization in the alveolus. *Nature*. 2020;586:785-789. https://doi.org/10.1038/s41586-020-2822-7

76. Hamanaka K, Jian MY, Weber DS, Alvarez DF, Townsley MI, Al-Mehdi AB, King JA, Liedtke W and Parker JC. TRPV4 initiates the acute calcium-dependent permeability increase during ventilator-induced lung injury in isolated mouse lungs. *Am J Physiol Lung Cell Mol Physiol*. 2007;293:L923-32. https://doi.org/10.1152/ajplung.00221.2007

Journal Pre-proof

77. Zhong M, Wu W, Kang H, Hong Z, Xiong S, Gao X, Rehman J, Komarova YA and Malik AB. Alveolar Stretch Activation of Endothelial Piezo1 Protects Adherens Junctions and Lung Vascular Barrier. *Am J Respir Cell Mol Biol*. 2020;62:168-177. https://doi.org/10.1165/rcmb.2019-0024OC

78. Su G, Hodnett M, Wu N, Atakilit A, Kosinski C, Godzich M, Huang XZ, Kim JK, Frank JA, Matthay MA, Sheppard D and Pittet JF. Integrin alphavbeta5 regulates lung vascular permeability and pulmonary endothelial barrier function. *Am J Respir Cell Mol Biol*. 2007;36:377-86. https://doi.org/10.1165/rcmb.2006-0238OC

79. Zielinski JL, Lee CH, Gunatilaka A, Gao B and Stewart AG. Mechanopharmacology: in vitro techniques to advance drug discovery. *Br J Pharmacol*. 2024. https://doi.org/10.1111/bph.17401

Journal Pre-proof

Figures and figure legends

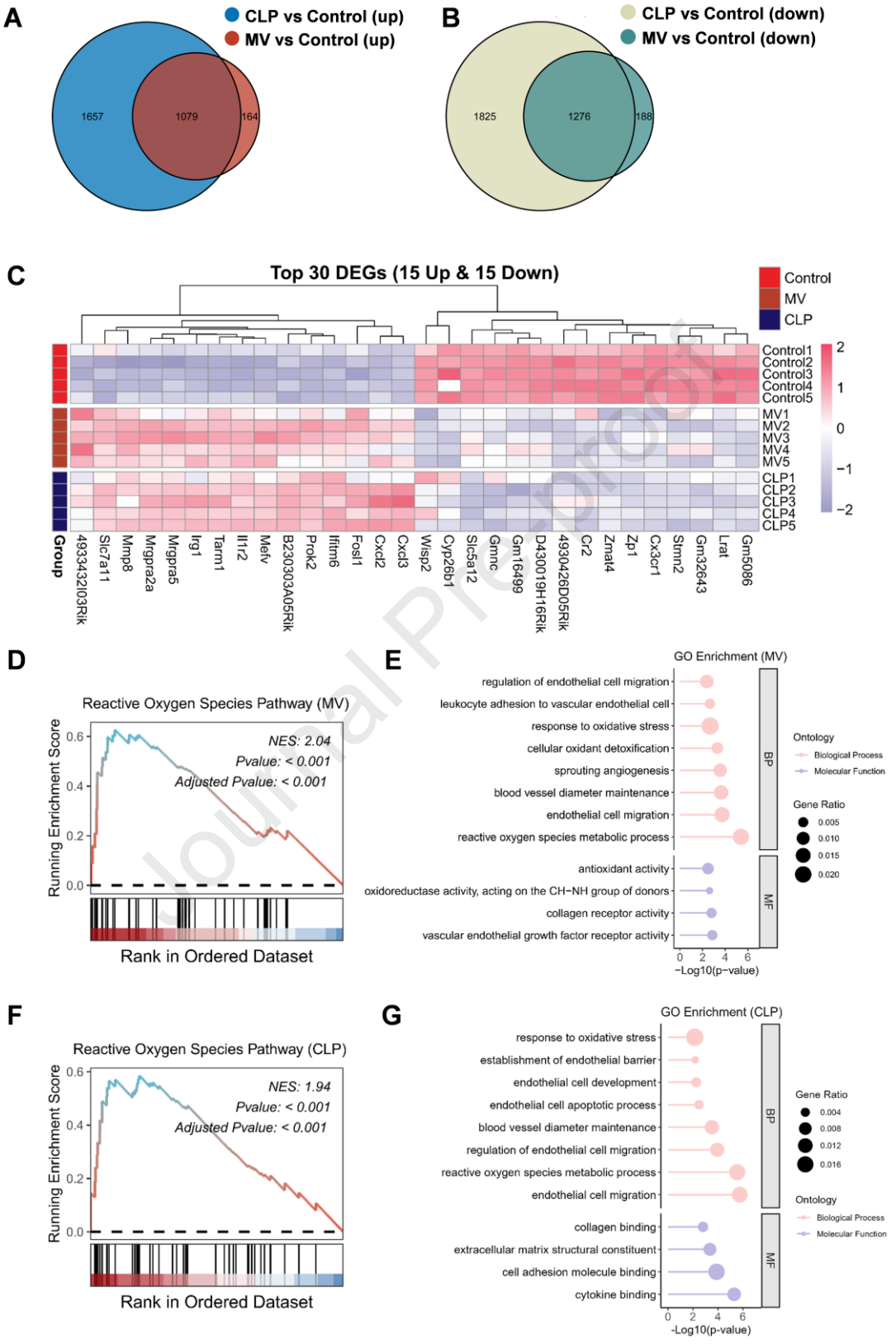

Figure 2. Gene expression profiling in MV- and CLP-induced lung injury.

(**A**) The Venn diagram highlights genes commonly upregulated in CLP and MV

groups compared to their respective controls. (**B**) The Venn diagram identifies overlapping downregulated genes in the CLP and MV groups compared to their respective controls. (**C**) The heatmap visualizes the expression profiles of the top 15 upregulated and 15 downregulated genes in the MV group versus controls, as well as these genes' expression levels in the CLP group compared to its respective controls. (**D**) GSEA plot shows altered ROS signaling pathway activity in lung tissue of the MV group. (**E**) GO analysis highlights the significant enrichment of differential expressed genes in oxidative stress-related and endothelial function regulation pathways in the MV group. (**F**) GSEA plot demonstrates alterations in ROS signaling pathway activity in CLP group lung tissue. (**G**) GO analysis reveals significant enrichment of differentially expressed genes in the CLP group, particularly in pathways associated with oxidative stress and endothelial function regulation.

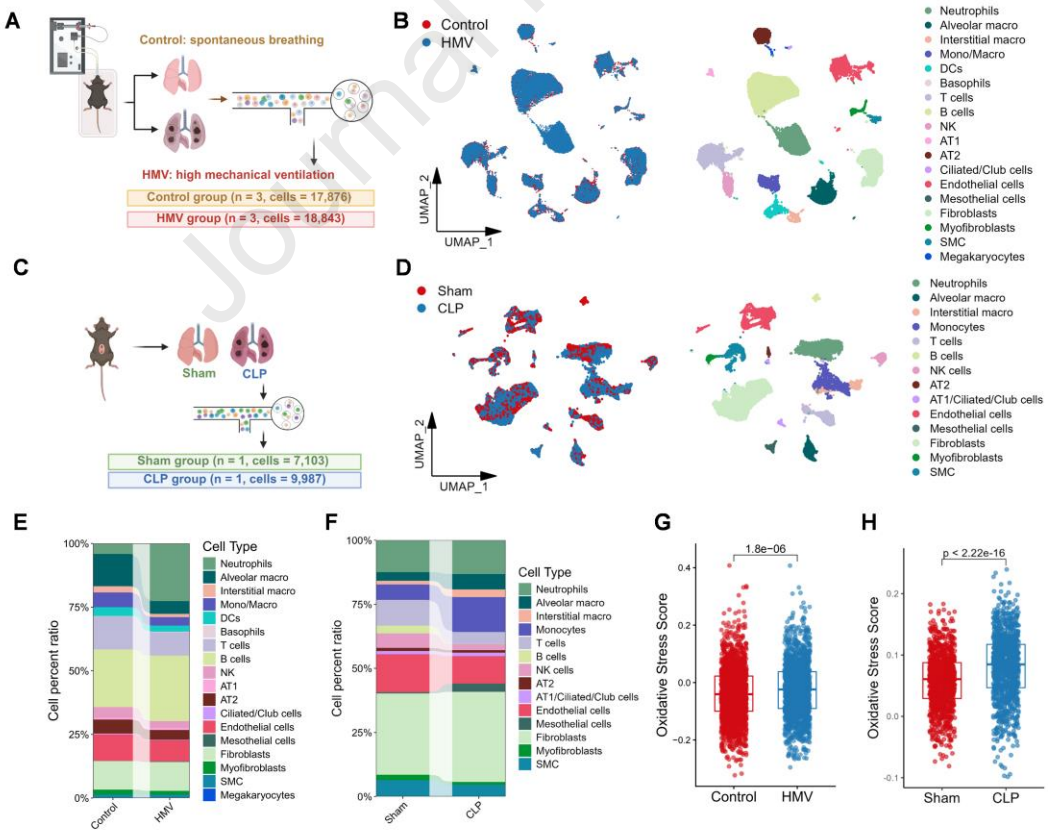

Figure 3. ScRNA-seq analysis reveals oxidative stress dynamics in lung endothelial cells during MV- and CLP-induced lung injury. A. Schematic

diagram illustrating the scRNA-seq workflow applied to the H-MV-induced lung injury model. Lung tissues from 3 control mice and 3 H-MV-treated mice were dissociated into single-cell suspensions. Unsorted cells were processed using the 10× Genomics Chromium platform for scRNA-seq library construction. **B**. UMAP plot of scRNA-seq data showing 18 major cell clusters in H-MV-induced lung injury scRNA-seq data, annotated with lineage-specific markers. **C**. Schematic overview of the scRNA-seq workflow applied to the CLP-induced lung injury dataset (GSE207651). **D**. UMAP plots showing 14 major cell types identified in CLP-induced lung injury scRNA-seq data. **E-F**. Stacked bar plots illustrating proportional changes of major cell populations in H-MV (**E**) and CLP (**F**) models relative to controls. **G-H**. Bar plots quantifying oxidative stress scores in lung endothelial cells from H-MV-treated (**G**) and CLP-treated (**H**) mice, demonstrating differential stress responses.

Journal Pre-proof

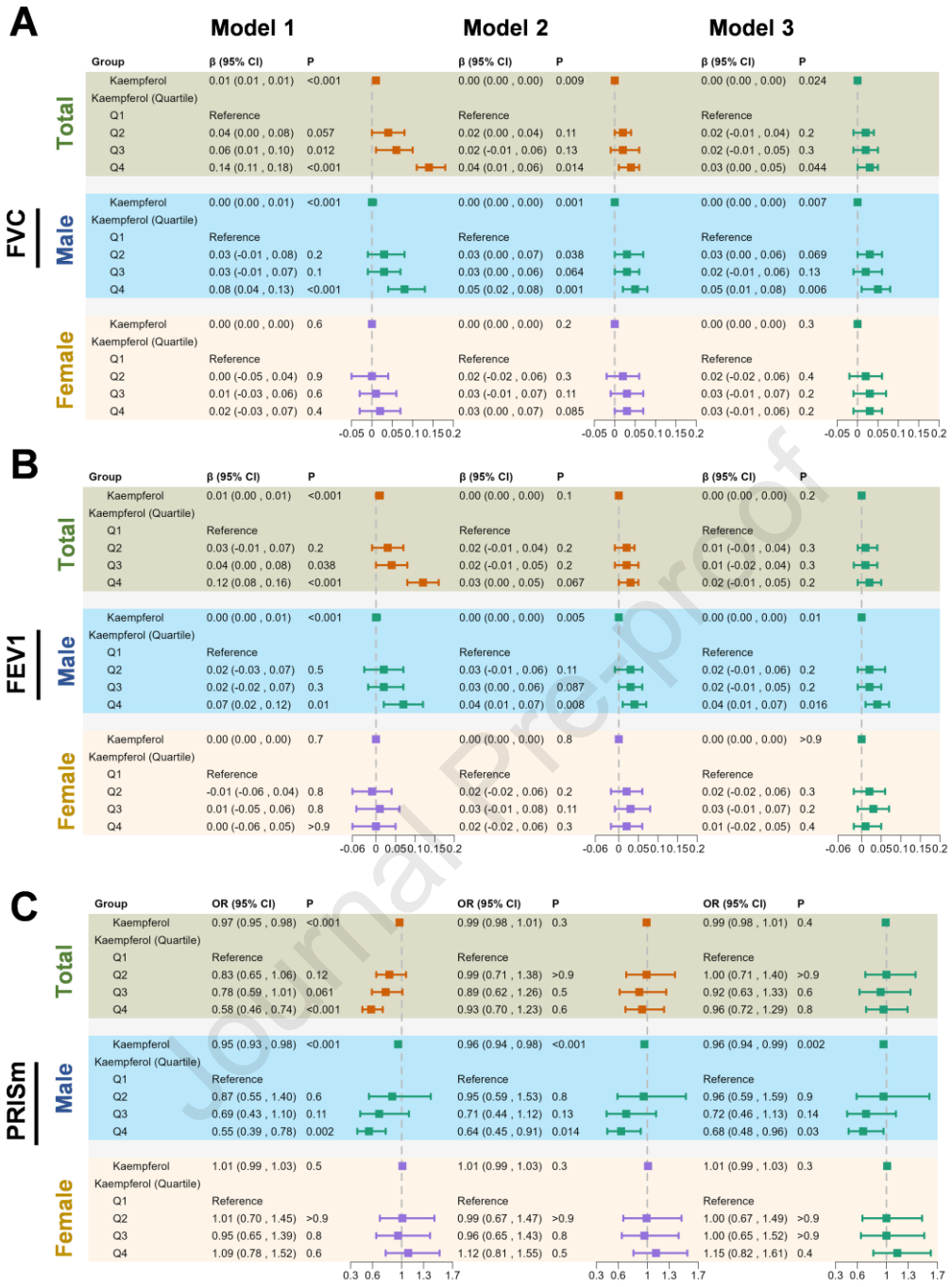

Figure 4. Associations between kaempferol and the prevalence of forced vital capacity (FVC), forced expiratory volume in one second (FEV1) and preserved ratio but impaired spirometry (PRISm). **A-B**. Multiple linear regression demonstrates the association between continuous kaempferol, its quartiles, and FVC (**A**) and FEV1 (**B**). **C.** Multinomial logistic regression demonstrates the association between continuous kaempferol, its quartiles, and PRISm. Model 1, unadjusted.; Model 2, adjusted for age, gender, race,

education level and FPIR; Model 3, adjusted for age, gender, race, education level, FPIR, BMI, smoking, drinking, hypertension status, diabetes status, hyperlipidemia status. OR, odds ratio; CI, confidence interval.

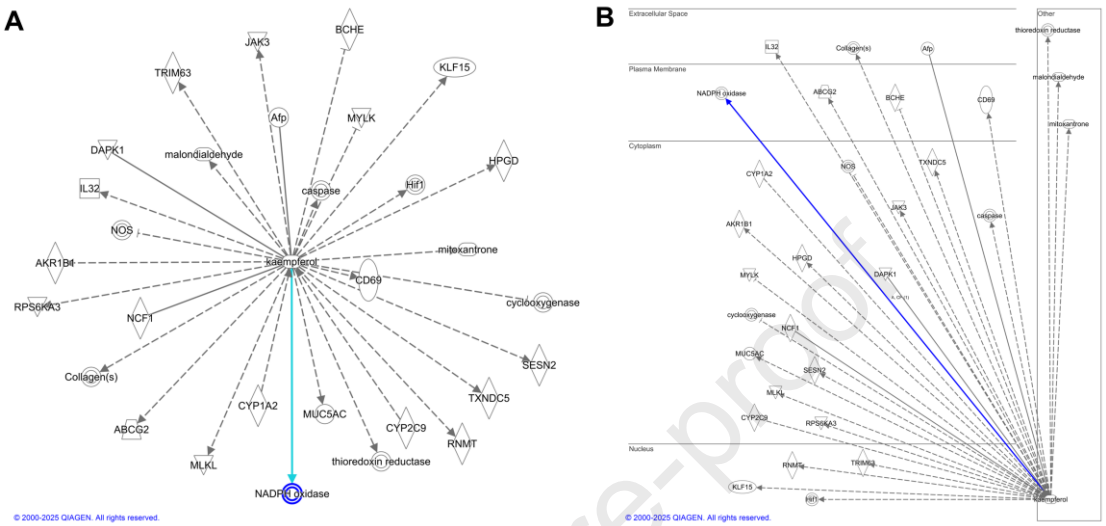

Figure 5. Functions and diseases related to kaempferol and the top 30 molecules targeted by kaempferol analyzed by Ingenuity Pathway Analysis (IPA). A. IPA was performed to identify molecules targeted by kaempferol. NOX was shown to be directly modulated by kaempferol, as indicated by the blue arrow. **B.** Subcellular localization of the top 30 molecules targeted by kaempferol**,** four of which are located in the plasma membrane. Of these four, only NOX is directly regulated by kaempferol as highlighted by the blue arrows. — (solid line) refers to a direct interaction; ..... (dotted line) refers to an indirect interaction. Straight line without arrowhead indicates undirected associations (e.g., chemical–chemical, protein–protein, RNA–RNA, or correlation-based interactions); ◎ indicates complex/group; ⬭ indicates chemical/toxicant; □ indicates cytokine; ◇ indicates enzyme; ▽ indicates kinase; ⏢ indicates transporter; ⬭ indicates transcriptional regulator; ⬯ indicates transmembrane receptor; ⬚ indicates growth factor.

Journal Pre-proof

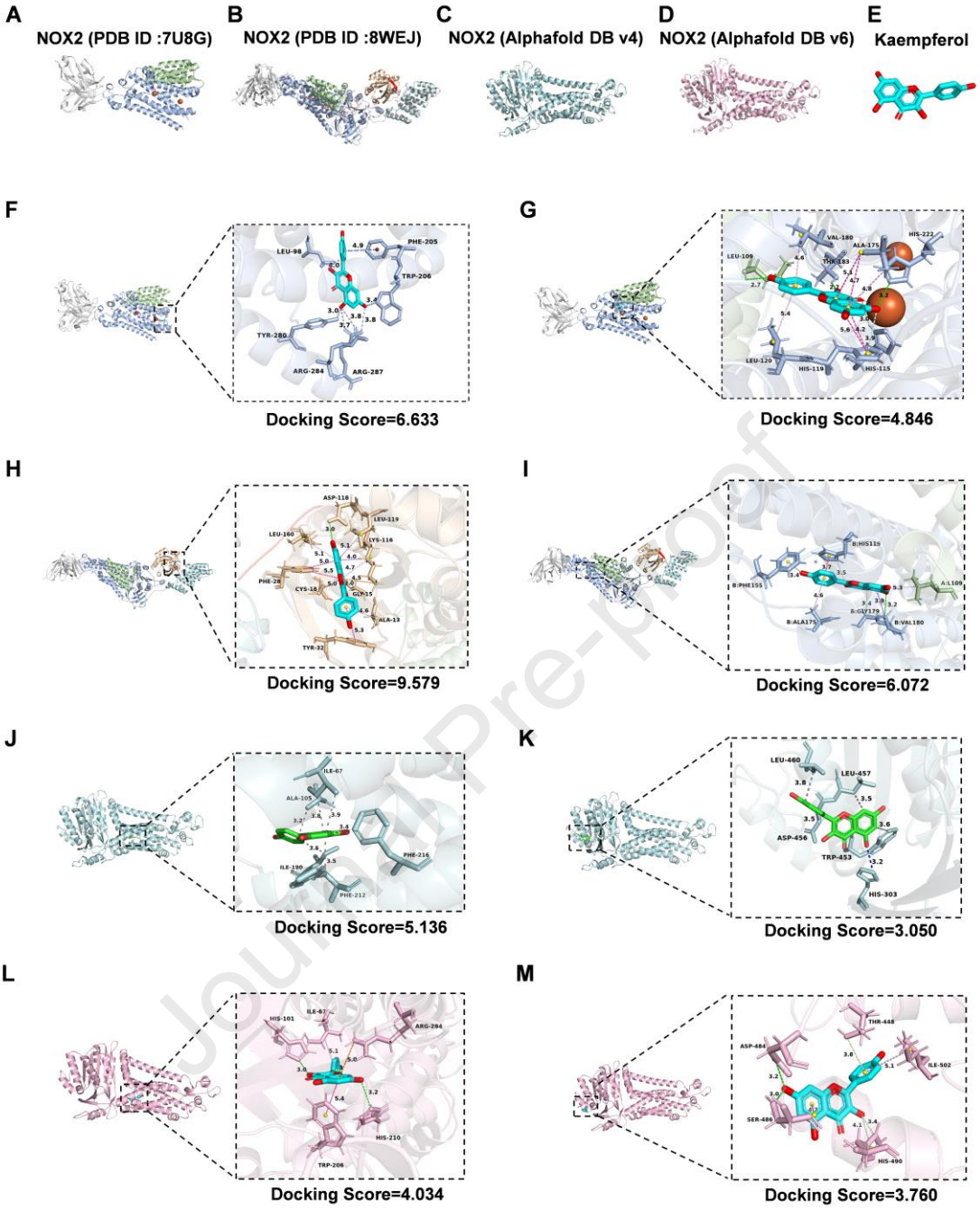

Figure 6. Molecular docking reveals potential interaction between kaempferol and NOX2. A. Cryo-EM structure of the activated NOX2 complex (PDB ID: 7U8G) used as the docking receptor. gp91^{phox} (chain A) is shown in blue, p22^{phox} (chain B) in green, and the antibody Fab heavy and light chains (chains C and D)—in gray. **B.** Cryo-EM structure of the activated NOX2 complex (PDB ID : 8WEJ) used as the docking receptor. gp91^{phox} (chain B) is shown in blue, p22^{phox} (chain A) in green, p47^{phox} (chain C) in red, p67^{phox} (chain D) in cyan, Rac1 (chain E) in golden, and the antibody Fab heavy and

light chains (chains F and G)—in gray. **C-D.** Two gp91phox structural models retrieved from the AlphaFold Protein Structure Database, DB v4 in (**C**), DB v6 in (**D**). **E.** Chemical structure of kaempferol. **F-G.** Two top-scoring docking poses on 7U8G; the highest-scoring pose (**F**) localizes to the $gp91^{phox}$, whereas the other pose (**G**) maps to the $p22^{phox}$-$gp91^{phox}$ region. **H-I.** Two top-scoring docking poses on 8WEJ after excluding conformations occupying the antibody-binding region; the highest-scoring pose (**H**) localizes to the Rac1 subunit, whereas the other pose (**I**) maps to the $p22^{phox}$-$gp91^{phox}$ region near the membrane-cytosol interface. **J-K.** Two representative top-ranked docking poses on the AlphaFold DB v4 $gp91^{phox}$ model. **L-M**. Two representative top-ranked docking poses on the AlphaFold DB v6 $gp91^{phox}$ model. Key proximal residues are displayed as sticks. Dashed lines indicate interatomic distances (Å).

Journal Pre-proof

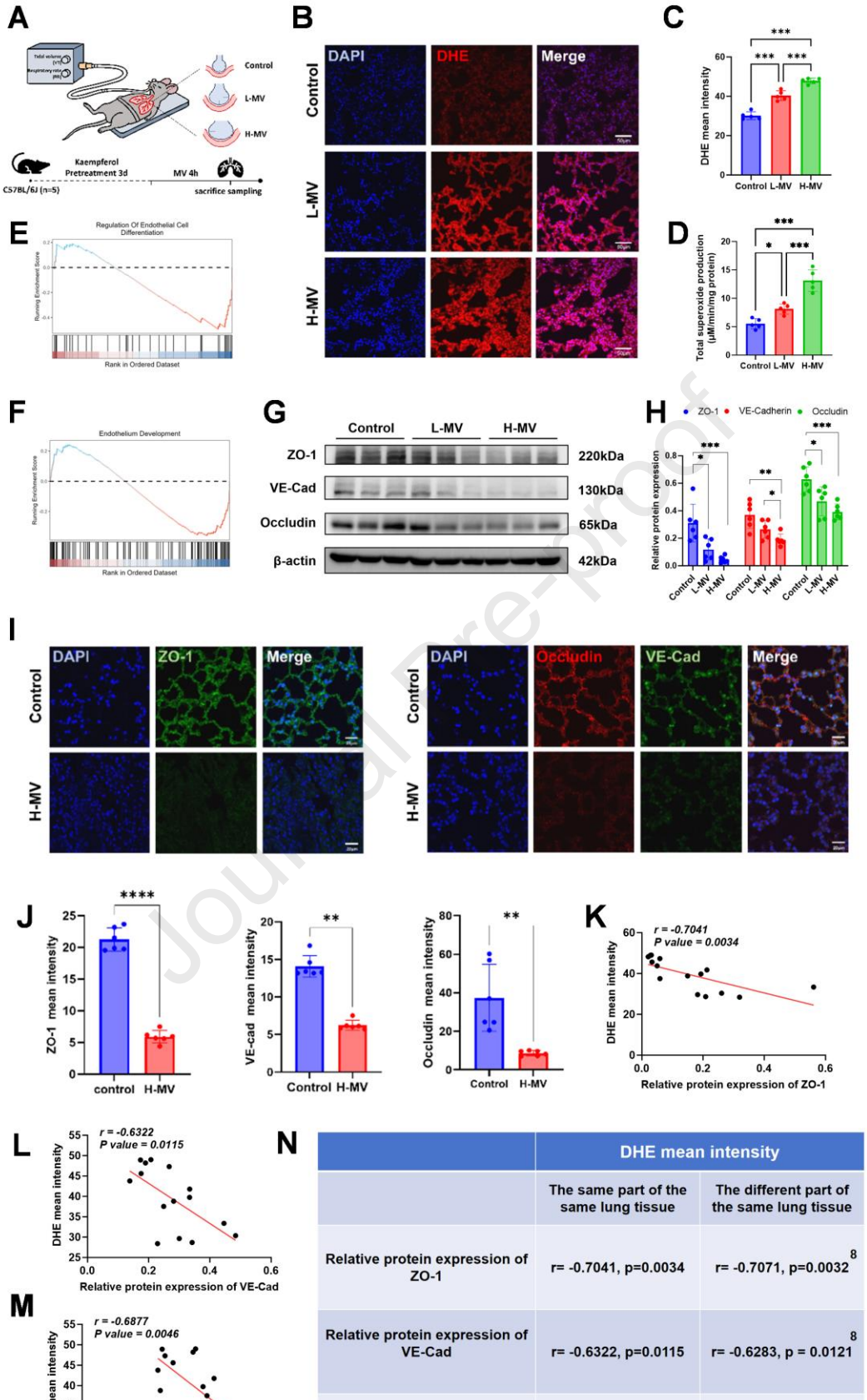

N

	DHE mean intensity	
	The same part of the same lung tissue	The different part of the same lung tissue
Relative protein expression of ZO-1	r= -0.7041, p=0.0034	r= -0.7071, p=0.0032[8]
Relative protein expression of VE-Cad	r= -0.6322, p=0.0115	r= -0.6283, p = 0.0121[8]
Relative protein expression of Occludin	r= -0.6877, p=0.0046	r= -0.8100, p=0.0085[8]

1

Figure 7. MV leads to ROS generation and endothelial dysfunction in various lung regions. A. Schematic diagram of the mouse MV model**. B-C.** Representative DHE fluorescent images in mice lung tissue sections (**B**), and the quantitative analysis (**C**) from the Control, L-MV, and H-MV groups. Scale bars: 50 μm. **D**.Total superoxide production was determined specifically and quantitatively by ESR spectroscopy in mice lung tissue from the Control, L-MV, and H-MV groups, n = 5. **E-F**. GSEA displays the changes in regulation of endothelial cell differentiation (**E**) and endothelium development (**F**) before and after MV in mice in GSE121550 datasets. **G-H**. Representative Western blot images (**G**), and the quantitative analysis (**H**) of protein expressions of ZO-1, VE-cadherin (VE-cad) and Occludin in lung tissue from the Control, L-MV, and H-MV groups. n = 6. **I-J**. Representative immunofluorescent images of ZO-1, Occludin and VE-cad (**I**), and the quantitative analysis (**J**) in mice lung tissue sections from the Control and H-MV groups. Nuclei were counterstained with DAPI. The average fluorescent intensity of ZO-1, Occludin and VE-cad was quantified using Image J software. Scale bars: 20 μm, n=6. **K-M**. Correlation analysis between DHE fluorescence intensity (ROS level) and relative protein expression of ZO-1 (**K**), VE-cad (**L**), and Occludin (**M**) within the same lung samples, n = 15. **N**. Summary table of correlation coefficients (r) and p-values between DHE fluorescence intensity and tight junction protein expression in the same and different regions from the same lung tissue. Data are presented as mean ± SD. *P < 0.05, **P < 0.01, ***P < 0.001 for the indicated comparisons.

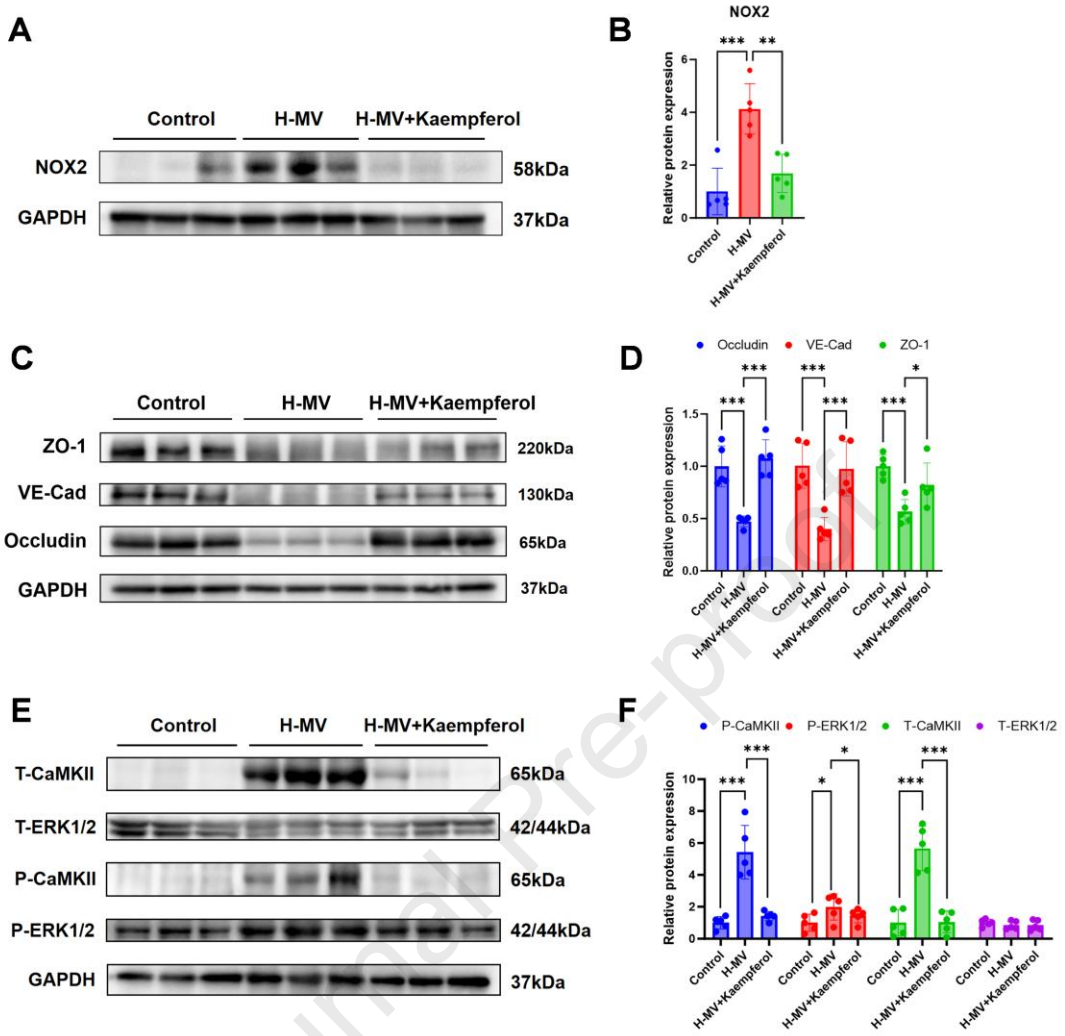

Figure 8. Kaempferol alleviates VILI by modulating NOX2/CaMKII/ERK1/2 signaling pathway. A-B. Representative Western blot images (**A**), and the quantitative analysis (**B**) of protein expressions of NOX2 in lung tissue homogenates from the Control, H-MV and H-MV + Kaempferol groups. n = 5. **C-D.** Representative Western blot images (**C**), and the quantitative analysis (**D**) of protein expressions of ZO-1, VE-Cad and Occludin in lung tissue homogenates from the Control, H-MV and H-MV + Kaempferol groups. n = 5. **E-F**. Representative Western blot images (**E**), and the quantitative analysis (**F**) of protein expressions of CaMKII and ERK1/2 in lung tissue homogenates from the Control, H-MV and H-MV + Kaempferol groups. n = 5. Data are presented as mean ± SD. *P < 0.05, **P < 0.01, ***P < 0.001.

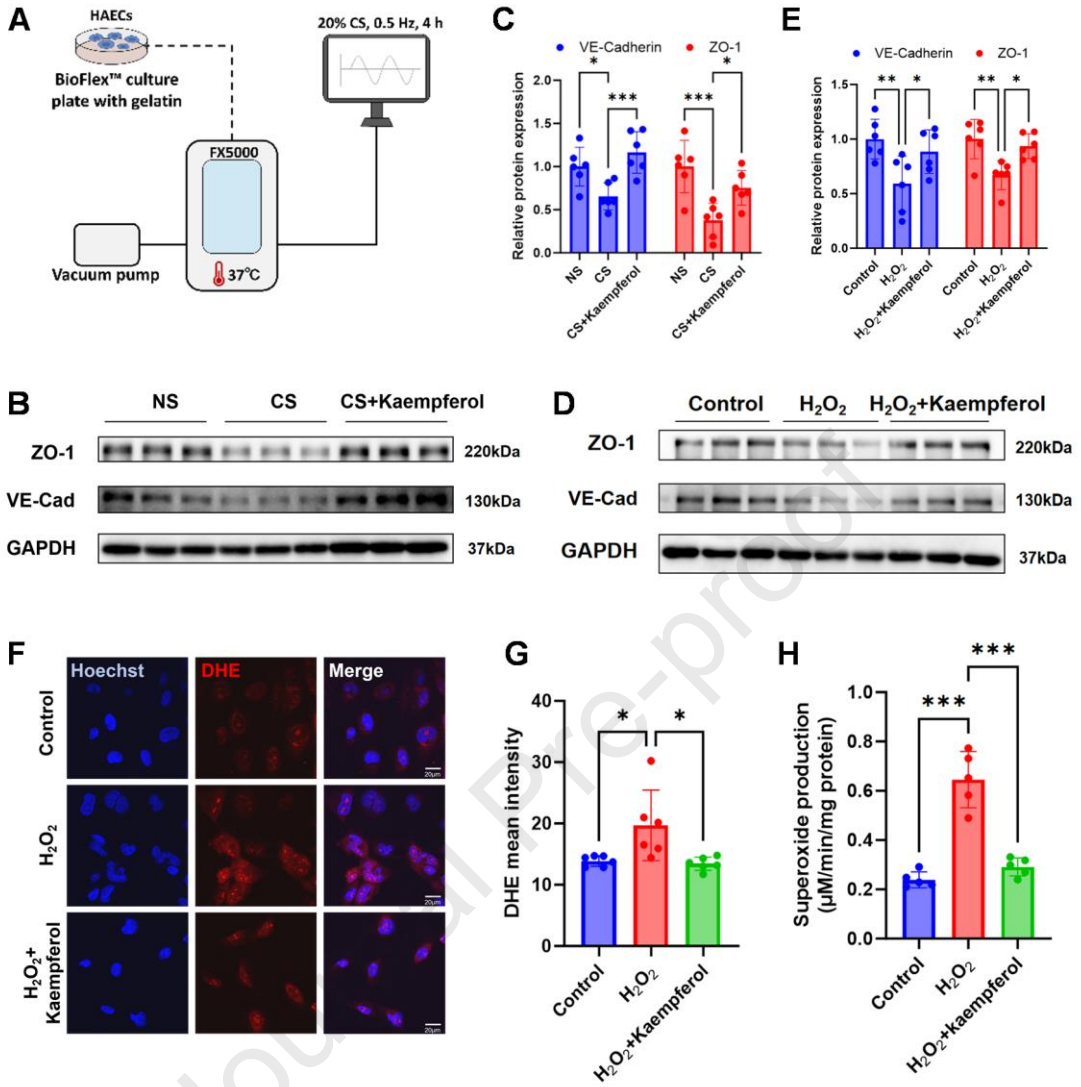

Figure 9. Kaempferol mitigates endothelial junction disruption induced by high cyclic stretch and hydrogen peroxide. A. Schematic diagram of the flexcell FX-5000 system, HAECs were subjected to cyclic stretch (CS) using this system in vitro. **B-C.** Representative Western blot images (**B**), and the quantitative analysis (**C**) of protein expressions of ZO-1 and VE-cadherin in HAECs from the non-stretch (NS), CS, and CS+Kaempferol groups. n = 6. **D-E.** Representative Western blot images (**D**), and the quantitative analysis (**E**) of protein expressions of ZO-1 and VE-cadherin in HAECs from the Control, H_2O_2, and H_2O_2+Kaempferol groups. n = 6. Data are presented as mean ± SD. *P < 0.05, **P < 0.01, ***P < 0.001. **F-G.** Representative DHE fluorescent images (**F**) and the quantitative analysis (**G**) in HAECs from the Control, H_2O_2,

and H_2O_2+Kaempferol groups. Scale bars: 20 μm. (**H**) Total superoxide production was determined specifically and quantitatively by ESR spectroscopy in HAECs from the Control, H_2O_2, and H_2O_2+Kaempferol groups, n = 5.

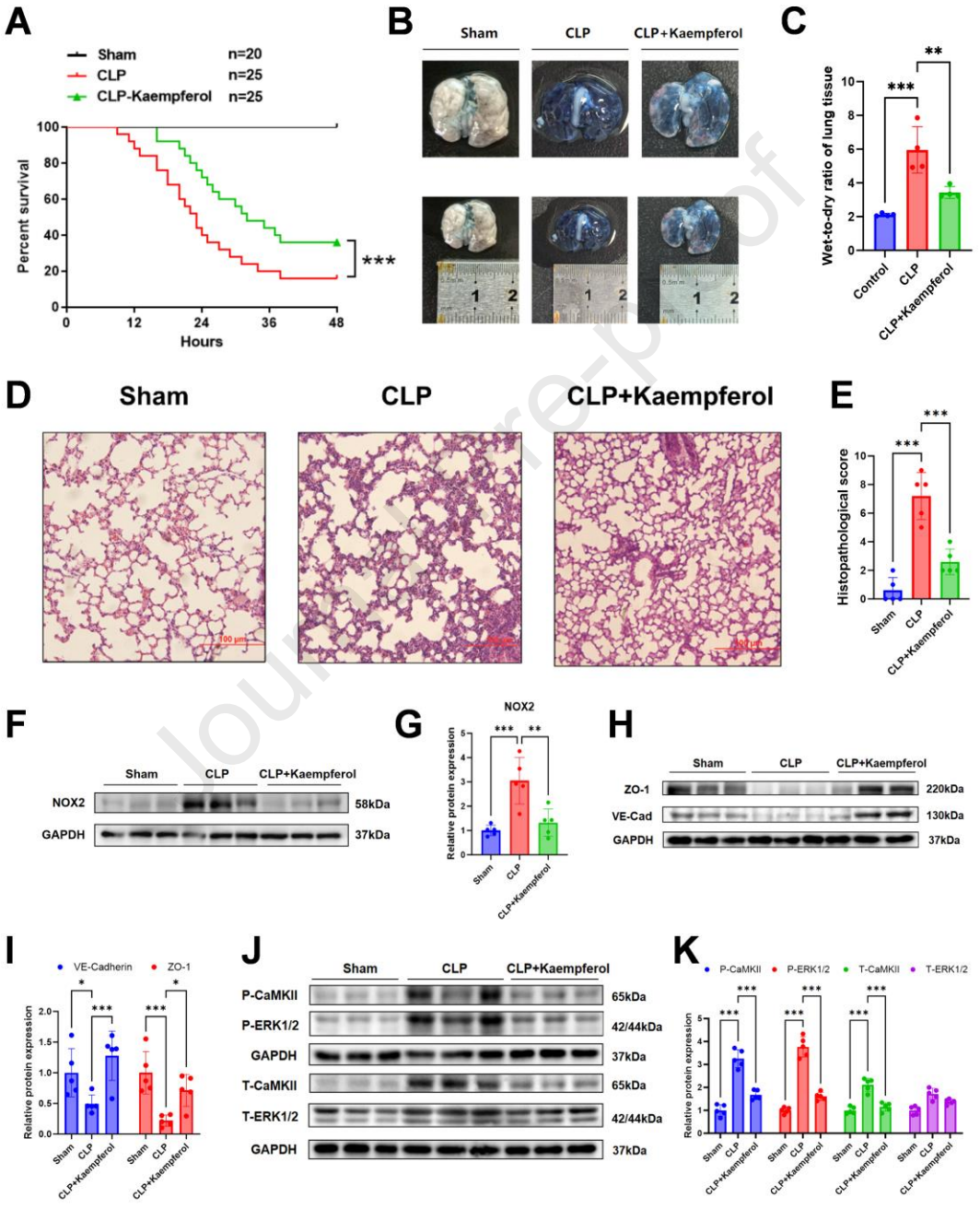

Figure 10. Kaempferol attenuates CLP-induced pathological injury by modulating the NOX2/CaMKII/ERK1/2 axis. A. Survival curves of mice subjected to Sham (n=20), CLP (n=25), or CLP+Kaempferol (n=25). **B.**

Representative images of Evans blue dye extravasation in lung tissues from Sham, CLP, and CLP+Kaempferol groups. **C.** Wet-to-dry (W/D) ratio of lung tissue in Sham, CLP, and CLP+Kaempferol groups. n = 4. **D-E**. Representative H&E images of mice lung tissue sections from the Sham, CLP, and CLP + Kaempferol groups (**D**), and the quantitative analysis of lung injury histological scores (**E**). Scale bars: 100 μm, n = 5. Data are presented as mean ± SD. **F-G**. Representative Western blot images (**F**), and the quantitative analysis (**G**) of protein expressions of NOX2 in lung tissue homogenates from the Sham, CLP, and CLP + Kaempferol groups. n = 5. **H-I**. Representative Western blot images (**H**), and the quantitative analysis (**I**) of protein expressions of ZO-1 and VE-Cad from the Sham, CLP, and CLP + Kaempferol groups. n = 5. **J-K**. Representative Western blot images (**J**), and the quantitative analysis (**K**) of protein expressions of ERK1/2 and CaMKII from the Sham, CLP, and CLP + Kaempferol groups. n = 5. Data are presented as mean ± SD. *P < 0.05, **P < 0.01, ***P < 0.001.

Journal Pre-proof

Journal Pre-proof

Dear Editorial Office,

I declare that this manuscript has no conflict to disclose.

Thank you so much for your time and kind consideration!

Warm regards,

Kai

Kai Huang, Ph.D.
Associate Professor
Institute of Mechanobiology & Medical Engineering, School of Life Sciences & Biotechnology, Shanghai Jiao Tong University,
800 Dongchuan Road, Minhang, 200240, Shanghai, China.
Email: huang_kai@sjtu.edu.cn.

Journal Pre-proof